

## ABSTRACT

AKAFIA, MARTIN. Kinetics and Mechanisms of Metal Hydroxide Dissolution promoted by Structurally Diverse Siderophores. (Under the direction of Owen Duckworth.)

Iron is an abundant element in soils and sediments that is essential for all living organisms. However, because of its slow dissolution kinetics and low solubility, iron is usually not bioavailable to most microbes and plants in aerobic systems. In response to low bioavailability, organisms produce and exude siderophores, a class of biogenic chelating agents that have a high affinity for and facilitate the uptake of metals by graminaceous plants, bacteria, and fungi. In addition, siderophores may be exuded in concert with small organic acids, which may increase the effectiveness of siderophores in solubilizing iron and other metals. Although siderophores have historically been thought of as being specific for Fe(III), recent studies have demonstrated the formation of high affinity complexes with other environmentally and biologically relevant metals, including Mn, Co, Ni, V, and Mo. These observations suggest that siderophores may play important roles in the cycling of a variety of trace metals in the environment. Siderophores exhibit great structural diversity, but most studies of non-ferric metal-siderophore interactions have focused on a small number of these structures. This study utilized three different siderophores with properties that span the known structural diversity to examine the siderophore-promoted dissolution rates of FeOOH, CoOOH, and MnOOH in the absence and presence of the low molecular mass organic acid oxalate by utilizing batch dissolution experiments at pH from 5 to 9. Metal-siderophore complex concentrations as well as total metal dissolved concentrations were measured from experimental periods of one hour to fourteen days, depending on metal hydroxide and pH of experiments. The results show that

MnOOH and CoOOH generally dissolve more quickly in the presence of siderophores than FeOOH. Whereas FeOOH dissolved exclusively by ligand-promoted dissolution, MnOOH and CoOOH dissolved predominantly by reductive dissolution under most experimental conditions. For MnOOH and FeOOH, dissolution rates trended with aqueous stability constants. In the presence of oxalate, siderophore-promoted dissolution rates may increase, decrease, or be unaffected as compared to rates in the presence of siderophores alone, depending on pH, siderophore, and metal hydroxide identity. These results bracket the possible dissolution reactivity of siderophores with both ferric and non-ferric hydroxide minerals in the environment, and may provide basic insights into how siderophores can be utilized in remediation of metal impacted sites.

Kinetics and Mechanisms of Metal Hydroxide Dissolution promoted by Structurally Diverse  
Siderophores

by  
Martin Akafia

A thesis submitted to the Graduate Faculty of  
North Carolina State University  
in partial fulfillment of the  
requirements for the degree of  
Master of Science

Soil Science

Raleigh, North Carolina

2013

APPROVED BY:

---

Owen Duckworth  
Committee Chair

---

Matthew Polizzotto

---

Christopher Osburn

---

Dean Hesterberg

## **BIOGRAPHY**

Martin Akafia was born and raised in Accra and Tema, Ghana as the first of four siblings, a brother and two sisters. After graduating from high school, he pursued a two year diploma in Information Technology before moving on to study Geology at the University of Ghana. Prior to his undergraduate studies in geology, he had developed software for Vlisco Ghana Ltd a multinational company that manufactured textile products. By his second year in the university he had set up an IT firm with his friend from high school and now a medical doctor, Anthony Bandoh specializing in software development, graphic design and internet services employing 5 people. Despite the time this took from his studies, he graduated with a BSc degree in geology. After 7 years running the company he decided to shift focus to work with a land development firm but after one year decided to pursue higher education. In December 2007 he moved to Kalamazoo, Michigan to start a master's degree program in geology and graduated officially in December 2010 from Western Michigan University. He however started a PhD program at NC State in August 2010 but after a series of personal misfortunes decided to finish off with a master's degree. He wants to continue his career as an environmental consultant after the completion of his program.

## ACKNOWLEDGEMENTS

I would first of all like to acknowledge my advisor, Dr. Owen Duckworth for giving me this opportunity and for standing by me during the most difficult time period in my life. His strong dedication to research, depth of knowledge, insight and quick response to questions and laboratory logistical issues has been particularly helpful in moving this project forward.

I am particularly grateful to the National Science Foundation for making this research possible as well as to the Graduate College of North Carolina State University. I would also like to show my appreciation to members of my committee, Dr. Dean Hesterberg, Dr. Matthew Polizzotto and Dr. Christopher Osburn for their advice and suggestions on various aspects of this thesis. I am also indebted to Dr. Jot Smyth, Dr. Michael Waggoner, Dr. Joseph Kleiss, Dr. Wei Shi, Ms. Dee Ann Cooper, and the Soil Science faculty as a whole for their help in various ways throughout my study here.

To my parents and siblings for their support and prayers. I also want to thank my wife Shante for all her strong support and encouragement as well as sacrifices to keep this dream alive and to my sons Mawuena and Sena “*Omnia Vincit labor*”. Finally I want to thank the Soil Biogeochemistry group Dr. James Harrington, Dr. Megan Andrews, Dr. Navdeep Kaur, Dr. Terrence Gardner, Dr. Nelson Rivera, Dawn Makarian, Kate Kubolk, Tyler Sowers, Tyler Johnston and Zach Collins for their help in various ways in and out of the lab. Kim Hutchison and Mr. Ramirez from the service lab for their help in analyzing some of my samples.

## TABLE OF CONTENTS

LIST OF TABLES .....	vi
LIST OF FIGURES .....	vii
Chapter 1 .....	1
1.1 Introduction.....	2
1.2 Siderophores .....	3
1.3 Chemistry of Siderophore Metal Interactions.....	5
1.4 Metal Hydroxides in the Environment.....	6
1.4.1 Iron Hydroxides.....	6
1.4.2 Cobalt Hydroxide .....	7
1.4.3 Manganese Hydroxide.....	8
1.5 Metal Hydroxides Surface Reactivity.....	9
1.5.1 Surface Chemistry and Adsorption Reactions .....	9
1.5.2 Dissolution Mechanisms .....	10
1.5.3 Non-Reductive ligand-promoted dissolution .....	11
1.5.4 Reductive Dissolution .....	12
1.5.5 Proton Promoted Dissolution .....	12
1.6 Siderophore-Promoted Dissolution Minerals .....	13
1.6.1 Iron Minerals .....	13
1.6.2 DFOB-Promoted Dissolution of Metal Oxides.....	14
1.6.3 Siderophore-Promoted Mineral Dissolution in the Presence of Low Molecular Mass Organic Acids.....	15
1.7 Summary .....	16
1.8 References.....	18
Chapter 2.....	29
Siderophore Promoted Dissolution of FeOOH, MnOOH, and CoOOH in the Presence and Absence of Oxalate .....	29
2.1 Introduction.....	30
2.2 Materials and Methods.....	32
2.2.1 Reagents .....	32
2.2.2 Siderophores.....	33
2.2.3 Synthesis of metal hydroxides.....	33

2.2.4 Particle characterization .....	34
2.2.5 Siderophore-promoted dissolution of goethite, heterogenite, and manganite.....	35
2.2.6 Dissolution of goethite, heterogenite and manganite in the presence of oxalate and siderophores .....	36
2.2.7 Quantification of dissolved siderophore complexes .....	38
2.2.8 Atomic absorption spectrometry .....	38
2.2.9 Quantification of dissolution rates .....	39
2.3 Results and Discussion .....	40
2.3.1 Trends in Siderophore-promoted Dissolution Rates for Metal Oxide. ....	40
2.3.2 Siderophore-promoted dissolution of FeOOH. ....	41
2.3.3 Siderophore-promoted dissolution of CoOOH and MnOOH .....	44
2.3.4 Siderophore-promoted dissolution rates of metal hydroxides in the presence of oxalate. ....	46
2.4 Summary and Conclusion .....	48
2.5 References.....	50
Chapter 3.....	75
Summary and Conclusions .....	75
3.1 Summary of Findings.....	76
3.2 Broader Implications of Major Findings.....	77
3.3 Final Thoughts .....	78
3.4 References.....	80
APPENDIX.....	81

## LIST OF TABLES

Table 1.1 Stability constants of metal-HDFOB complexes.....	28
Table 2.1 Beer-Lambert extinction coefficients at specific wavelengths for metal-siderophore complexes. ....	57
Table 2.2 Total dissolution ( $R_T$ ) and ligand-promoted ( $R_L$ ) dissolution rates for FeOOH. Conditions: 0.2 g L <sup>-1</sup> FeOOH; 100 μM siderophore; 25°C; 10 mM buffer; 0.1 M NaCl. ....	66
Table 2.3 Total initial dissolution rates ( $R_T$ in mol m <sup>-2</sup> s <sup>-1</sup> ) for FeOOH as promoted by DFOB and other siderophores at pH = 6. ....	67
Table 2.4 Total dissolution ( $R_T$ ) and ligand-promoted ( $R_L$ ) dissolution rates for MnOOH. Conditions: 0.2 g L <sup>-1</sup> MnOOH; 100 μM siderophore; 25°C; 10 mM buffer; 0.1 M NaCl. ND = not detected. ....	68
Table 2.5 Total dissolution ( $R_T$ ) and ligand-promoted ( $R_L$ ) dissolution rates for CoOOH. Conditions: 0.2 g L <sup>-1</sup> CoOOH; 100 μM siderophore; 25°C; 10 mM buffer; 0.1 M NaCl. ND = not detected. ....	69
Table 2.6 Total siderophore-promoted ( $R_T$ ) dissolution rates for FeOOH, CoOOH, and MnOOH in the presence of oxalate ( $R_{S_{ox}}$ ). Conditions: 0.2 g L <sup>-1</sup> MnOOH; 100 μM siderophore; 0 or 1000 μM oxalate; 25°C; 10 mM buffer; 0.1 M NaCl. ....	73
Table 2.7 Enhanced siderophore promoted total dissolution rates for FeOOH, CoOOH, and MnOOH in the presence of oxalate ( $R_{S_{ox}}$ ). Conditions: 0.2 g L <sup>-1</sup> MnOOH; 0 or 100 μM siderophore; 1000 μM oxalate; 25°C; 10 mM buffer; 0.1 M NaCl. ....	74

## LIST OF FIGURES

- Figure 1.1. Molecular structure of plant and bacterial siderophores showing structural diversity and functional groups..... 26
- Figure 1.2. Predominance diagram Showing Mn speciation different pH and Eh conditions. Figure is reproduced from (Stumm and Morgan, 1996). ..... 27
- Figure 2.1. Schematic showing the siderophores selected for use in this study. The siderophores were chose to span the structural diversity of bacterial siderophores. .... 56
- Figure 2.2. Dissolution of FeOOH as promoted by DFOB. Conditions: pH = 5; 0.2 g L<sup>-1</sup> FeOOH; 100 μM DFOB; 25°C; 10 mM acetate buffer; 0.1 M NaCl solution. Error bars present represent standard deviation of the mean. .... 58
- Figure 2.3. Dissolution of FeOOH as promoted by DFOB and oxalate. The experiment began with 1 mM oxalate (circles) and DFOB was added on the fourth day (triangles) Conditions: pH = 5; 0.2 g L<sup>-1</sup> FeOOH; 100 μM DFOB; 25°C; 10mM acetate buffer; 0.1 M NaCl solution. .... 59
- Figure 2.4. Logarithm of total initial dissolution rates coefficients for the siderophore-promoted dissolution of metal hydroxides. Conditions: 0.2 g L<sup>-1</sup> MOOH; 100 μM siderophore; 25°C; 10 mM buffer; 0.1 M NaCl. Rates are also tabulated in Table 2.2. .... 60
- Figure 2.5. Average ligand-promoted (R<sub>L</sub>) (open symbol) and total (R<sub>T</sub>) (closed symbols) dissolution rates for FeOOH as promoted by DFOB, rhizoferrin, and protochelin. Conditions: 0.2 g L<sup>-1</sup> FeOOH; 100 μM siderophore; 25°C; 10 mM buffer; 0.1 M NaCl solution. Error bars represent 95% confidence intervals. .... 61
- Figure 2.6. Plot of log stability constant and log dissolution rates of FeOOH (squares) and MnOOH (circles) as promoted by siderophores used in this study and from literature at pH 6. (Cocozaa, 2002; Neubauer, 2002; Lloyd 1999; Carrasco, 2009; Wolff-Boenisch and Traina, 2007; Reichard, 2007; Cervini-Silva, 2008; Harrington et al, 2012; Dubme et al., 1997). .... 62
- Figure 2.7. Average dissolution rates for MnOOH as promoted by DFOB, rhizoferrin, and protochelin. Conditions: 0.2 g L<sup>-1</sup> MnOOH; 100 μM siderophore; 25°C; 10 mM buffer; 0.1 M NaCl. Error bars represent 95% confidence interval. .... 63

Figure 2.8. Average dissolution rates for CoOOH tested at 95% confidence interval as promoted by DFOB, rhizoferrin, and protochelin. Conditions: 0.2 g L<sup>-1</sup> CoOOH; 100 μM siderophore; 25°C; 10 mM buffer; 0.1 M NaCl. .... 64

Figure 2.9. Trends in siderophore promoted dissolution rates for MnOOH, CoOOH and FeOOH as promoted by DFOB, rhizoferrin, and protochelin. MnOOH and CoOOH exceed FeOOH dissolution. Conditions: 0.2 g L<sup>-1</sup> CoOOH; 100 μM siderophore; 25°C; 10 mM buffer; 0.1 M NaCl..... 65

Figure 2.10. Average dissolution rates for FeOOH as promoted by DFOB with and without the presence of oxalate. Conditions: 0.2 g L<sup>-1</sup> FeOOH; 100 μM siderophore; 1000 μM oxalate; 25°C; 10 mM buffer; 0.1 M NaCl. Error bars represent 95% confidence intervals. . 70

Figure 2.11. Average dissolution rates for FeOOH as promoted by rhizoferrin with and without the presence of oxalate. Conditions: 0.2 g L<sup>-1</sup> FeOOH; 100 μM siderophore; 1000 μM oxalate; 25°C; 10 mM buffer; 0.1 M NaCl. Error bars represent 95% confidence intervals..... 71

Figure 2.12. Average dissolution rates for FeOOH as promoted by protochelin with and without the presence of oxalate. Conditions: 0.2 g L<sup>-1</sup> FeOOH; 100 μM siderophore; 1000 μM oxalate; 25°C; 10 mM buffer; 0.1 M NaCl. Error bars represent 95% confidence intervals..... 72

## **Chapter 1**

## 1.1 Introduction

Microbes form a vital link between the biotic and abiotic components of ecosystems. They are ubiquitous in both terrestrial and marine environments, and play very important ecological roles in controlling the biogeochemical cycling of elements that are essential for organism nutrition. It has been observed that biogenic ligands, exuded by both microbes and plants, may partially control the speciation of many metals, such as iron, cobalt and manganese, in terrestrial environments (Stone and Marsalek, 1996). These changes in speciation may in turn greatly alter the fate, transport, and bioavailability of both nutrient and contaminant metals.

Trace metals are essential for the metabolic function of all living cells. Iron is the most abundant transition metal in the enzymes of microbes and plants (Da Silva and Williams, 1991). It is frequently utilized in redox catalysis, including the electron transport chain, and serves as a vital nutrient in the nitrogen cycle via enzymes involved in the catalysis of nitrogen redox reactions (Vraspir, 2009). Nominal concentrations required for the growth of plants and microbes range from  $10^{-9}$  to  $10^{-4}$  M, and  $10^{-5}$  to  $10^{-7}$  M, respectively (Loper and Buyer, 1991; Römheld and Marschner, 1981; Schwab and Lindsay, 1983). Although iron constitutes about 5% of the Earth's crust, the activity of free dissolved ferric iron in oxic waters at circumneutral pH is restricted to  $>10^{-9}$  M by solubility constraints imposed by iron hydroxides, constraining Fe bioavailability in marine and terrestrial systems (Schwertmann and Cornell, 1991; Vraspir, 2009). Iron bioavailability and transport are further limited by slow dissolution kinetics of common iron minerals (Kraemer, 2003). This low bioavailability may limit biological production in both terrestrial and marine systems, and could affect the carbon fixation and

respiration on the global scale (Kraemer, 2004). In response to these limitations, microbes and plants have evolved strategies for obtaining iron by exuding organic compounds that increase its solubility and facilitate cellular uptake.

## **1.2 Siderophores**

Microbes exude low molecular weight organic complexing agents, known as siderophores, to facilitate the uptake of iron in environments where iron limits growth (Garibaldi and Neilands, 1956). Microbial growth factors that were later recognized as siderophores were first isolated by medical researchers over 100 years ago (Raymond, 1994; Twort and Ingram, 1912). By 1950, siderophores had been identified as microbial exudates with high affinities for iron complexation that can be efficiently taken up by organisms via specific transport across cell membranes (Garibaldi and Neilands, 1956; Hider and Kong, 2010). The term siderophore, which is the Greek word for “iron carrier”, has been adopted as a general term to refer to this class of ligands: however, they have historically been referred to by other names, including ferrichrome, ferrioxamines, siderochromes, and sideramines (Raymond, 1994).

To date, more than 500 different siderophores have been isolated. Although they are defined by biological function, they can be classified by common structural features. Most siderophores are tetradentate or hexadentate ligands containing various combinations of hydroxamate, carboxylate,  $\alpha$ -hydroxycarboxylate, and catecholate binding groups, and can be classified as linear, cyclic, or tripodal ligands (Boukhalfa and Crumbliss, 2002; Hider and Kong, 2010; Winkelmann, 2002). Examples of this structural diversity of microbial

siderophores, as well as those selected for inclusion in this thesis, are shown in Figure 1.1. In a limited number of reports describing siderophores in natural systems, their reported concentrations vary between  $10^{-11}$  to  $10^{-7}$  M in fresh water systems, soils, and the ocean (Duckworth et al., 2009c; Holmström and Kallio, 2004; Mucha et al., 1999). Although their concentrations are relatively low, their effectiveness comes from the high stability constants of Fe(III)-siderophore complexes, which range from  $10^{23}$  to  $10^{52}$  (Albrecht-Gary and Crumbliss, 1998). Of the different kinds, desferrioxamine B (DFOB; Figure 1.1), which has three hydroxamate functional groups, is the most studied siderophore, largely because it is commercially available, soluble, and represents the reactivity of siderophores in the trihydroxamate structural family.

As is implied by their name, siderophores were initially thought to have high specificity for iron binding and uptake. However, currently it is known that DFOB not only forms high affinity complexes with Fe(III), but also with other hard metal ions, such Co(III) and Mn(III) (Bi et al., 2010; Duckworth et al., 2009a; Duckworth et al., 2009b; Duckworth et al., 2009c). Additionally, recent work has demonstrated that catecholate and mixed-moiety siderophores may facilitate the active uptake of metals such as V and Mo (Batinic-Haberle et al., 1991; Baysse et al., 2000; Bellenger et al., 2008; Duhme-Klair, 2009; Duhme et al., 1996). This idea has led to the suggestion of new roles for siderophores in the transport and uptake of broader range of metals (Dosanjh and Michel, 2006; Duckworth et al., 2009b; Kraepiel et al., 2009a; Li and Zamble, 2009).

### 1.3 Chemistry of Siderophore Metal Interactions

Siderophore binding moieties have oxygen atoms that function as hard Lewis bases, interacting strongly with  $\text{Fe}^{3+}$  and other hard Lewis acids (Table 1). The common hexadentate siderophore form complexes by chelating the central metal ion ( $\text{Fe}^{3+}$ ) via five- or six-membered rings using the oxygen atoms as donor atoms (Lewis bases) in octahedral coordination, thereby allowing six moieties to be arranged around the iron center with minimum amount of ligand repulsion (Hider and Kong, 2010). The octahedral geometry allows the formation of the thermodynamically stable 1:1 complex with the high-spin Fe(III). The stability of siderophore-metal complexes also depends on the type of siderophore and the complex it forms with the metal ion, as well as the pKa value of the binding moieties and the associated competition with protons.

For DFOB, it has been shown that the stability of the complex varies with the charge to size ratio of the metal ion (Duckworth et al., 2009a; Hernlem et al., 1996; Krufft et al., 2013), with several metals, including Co(III) and Mn(III), having affinities that are near or exceed the stability constant for Fe(III) (Table 1.1). Siderophores with different geometries and binding moieties have different affinity for Fe(III) (Hider and Kong, 2010). This structural variety of siderophores further implies that they may be able to bind other chemically hard metals with higher relative affinity than with Fe(III). For example, the stability constants of several siderophores have differing relative affinities for Mn(III) and Fe(III) (Duckworth and Sposito, 2005b; Harrington et al., 2012; Parker et al., 2004). A paucity of published data with other siderophores with different selected trace metals limits our understanding of how the various siderophore structures affect their reactivity for other hard metal ions.

A major route of formation for ferric siderophore complexes in the environment is thought to be the dissolution of iron hydroxide minerals (Kraemer, 2003). Significantly less is known about their ability to dissolve other metals from minerals (Duckworth et al., 2009b). This thesis will therefore focus on reactions of DFOB, protochelin, and rhizoferrin (Figure 1.1), siderophores with differing binding moieties, with iron, manganese, cobalt and the hydroxides mineral phases of these metals.

## **1.4 Metal Hydroxides in the Environment**

### *1.4.1 Iron Hydroxides*

Iron is an important micronutrient utilized by all living organisms and is ubiquitous in the environment. Iron oxide and hydroxide minerals are commonly found in soils and sediments in a wide variety of environments. They are important agents that effect the cycling of other solutes, redox state, and microbial community of terrestrial ecosystems. Minerals exist as many distinct phases, ranging from poorly crystalline ferrihydrites to crystalline phases like goethite and hematite (Cornell and Schwertmann, 2003). Goethite ( $\alpha$ -FeOOH) is the most common crystalline iron hydroxide in soils and sediments due to its high thermodynamic stability (Schwertmann and Taylor, 1989). Goethite has a distorted hexagonal close packing structure consisting of three short O-Fe bonds and three long Fe-OH bonds with four repeat formula units (Cornell and Schwertmann, 2003). When in contact with water, the goethite surface has two types of terminal hydroxyls- a bidentate hydroxo group and a monodentate aquo group that may protonate or deprotonate depending on solution pH (Ghose et al., 2008).

For the pH range commonly encountered in soils, the solubility of the bulk goethite in solution generally decreases with increasing pH.

#### *1.4.2 Cobalt Hydroxide*

Cobalt is an environmentally and biologically important trace metal that occurs in soils at concentrations ranging from 3–70 mg kg<sup>-1</sup> (Sparks, 2001). It is an essential micronutrient for all microbes and animals (Adriano, 2001). Co is found in two main oxidation states: a more soluble +II state, and a less soluble +III state which is found mainly as heterogenite (CoOOH) when occurring as a pure mineral phase. CoOOH has a brucite structure with layers of edge-sharing Co(III)oxohydroxo octahedral. The Co(III)HDFOB<sup>+</sup> has a stability constant that is approximately five orders of magnitude greater than that of the Fe(III)HDFOB<sup>+</sup> complex (Table 1.1) (Duckworth et al., 2009a; Farkas and Szabo, 2012).

Furthermore, it was demonstrated that DFOB promotes CoOOH dissolution via reductive pathway at pH between 5 and 7, and a non-reductive pathway at pH above 7, and that DFOB promoted dissolution of CoOOH occurred more rapidly than FeOOH (Bi et al., 2010; McArdell et al., 1998; Penn et al., 2001). Although there is not much information about the interaction of CoOOH with siderophores other than DFOB, the high Co(III)HDFOB<sup>+</sup> stability constant motivates additional study of the interactions between CoOOH and the other siderophores under consideration in this work.

### *1.4.3 Manganese Hydroxide*

Manganese is the third most abundant transition metal in the earth's crust. Mn is found in many oxidation states in natural systems, from -III to +VII (Stumm and Morgan, 1996). Mn(II), Mn(III) and Mn(IV) are the most important oxidation states, and their stability depends on the Eh and pH values of the biological and environmental systems where they occur (Stone and Morgan, 1984). For microbes and all animals, Mn is responsible for enzymatic activities involved with glucose metabolism and energy production.

Mn(II) is the most stable oxidation state, and can be biotically or abiotically oxidized to either Mn(III) or Mn(IV) (Tebo et al., 2005). The variable oxidation state enables Mn to form more than 30 different minerals (Post, 1999). Manganese oxides, typically containing in Mn(III) or Mn(IV) oxidation state, impact the chemistry of natural systems by oxidizing organic matter as well as other metal ions, such as Cr(III) to the toxic Cr(VI) (Bartlett, 1988; Graham et al., 1988). These minerals are a natural sink for a variety of metals, and are found co-precipitated with elements like Fe (Tebo et al., 2005). Dissolution of the common phase manganite (MnOOH) by DFOB has been shown to occur via a reductive pathway at low pH and a non-reductive pathway at high pH (Duckworth and Sposito, 2005b).

It has been suggested that, because of the abundance of Mn oxides and their strong and rapid interactions with siderophores, the presence of Mn may disrupt siderophore-mediated iron uptake (Duckworth et al., 2009a). Thus, we have a strong interest to measure the kinetics as well as understand the mechanics of its interactions with other siderophores under consideration in this thesis.

## **1.5 Metal Hydroxides Surface Reactivity**

### *1.5.1 Surface Chemistry and Adsorption Reactions*

The fate and transport of nutrient and toxic metals in soils and sediments is determined to a large extent by the chemical reactions that take place at the water-mineral surface in aqueous solution (Borch et al., 2009). These interactions also affect biological availability and geochemical cycling of the metals contained in hydroxide minerals in the environment (Ghose et al., 2008). Hydroxide minerals (in this case, MOOH, where M is a trivalent ion) bear highly reactive surface sites that affect the ordering of water molecules at their interface and are responsible for the retention of many classes of substances. The surfaces of oxides are therefore the location of many environmentally important chemical reactions (Dzombak and Morel, 1990; Sverjensky and Sahai, 1996). In aqueous solutions, hydrous oxide surfaces contain surface hydroxyl or aquo functional groups that are subject to protonation and deprotonation (Stumm, 1997), resulting in the pH-dependent charge of minerals (Schaller et al., 2009). The combination of mineral surface, type and number of surface functional groups, the bond distance relaxation at the surface, the environment in which the mineral resides, and the valence and coordination of the structural metal atoms, are all factors that determine the reactivity of hydrous oxides (Brown Jr et al., 1999). The surface hydroxyl groups can exhibit both Lewis acid and Lewis base character in aqueous environments (Lund et al., 2008; Stumm and Morgan, 1996), binding with both cations and organic and inorganic ligands from solution. In an atomistic view, surface complexes are formed by exchange processes. The combination of surface structural sites and homogeneous solution speciation leads to the formation of a distinct set of surface species, each with specific chemical structure and reactivity at the mineral

surface. Non-specific adsorption occurs when ion-pair surface complexes are formed and maintained by electrostatic bonding (Drever, 1997; Stumm and Morgan, 1996). This type of surface complex can be easily dissociated because there is no specific bond between the hydroxyl group and adsorbed species. Inner-sphere complexes are formed if aqueous species bind directly to the surface with no intervening water molecules. This specific adsorption mechanism creates surface bonds of a relatively high degree of structural stability and configuration as well as some covalent character, making surface complexes harder to dissociate.

Additionally, direct bonds between an absorbing anion and a surficial metal ion may polarize the bonds between the surficial ion and the bulk mineral lattice, weakening the bonds that hold the ion to the surface. This type of association may control reactivity at the metal-solution interface such that a mononuclear multidentate complexation would more than likely favor mineral dissolution reactions (Bondietti et al., 1993; Duckworth and Martin, 2001; Furrer and Stumm, 1986). Understanding sorption behavior is critical to the interpretation of dissolution data because dissolution rates are typically directly related to the concentration of active surface sites.

### *1.5.2 Dissolution Mechanisms*

The dissolution of metal oxides may occur via several different reactions, including ligand-promoted, reductive, and proton-promoted pathways. The overall dissolution rate is typically assumed to be the sum of reaction rates for separate pathways that occur in parallel, although synergistic interactions are also possible.

### 1.5.3 Non-Reductive ligand-promoted dissolution

Biogenic ligands can promote dissolution of metal oxide minerals. If inner sphere surface complexes formed through adsorption reactions facilitate the dissolution of metals from the surface to the adjacent solution, the dissolution rates of oxides typically increase. The dissolution mechanism is usually expressed by the following three steps (Stumm, 1997):

- Fast adsorption of ligands on oxide surface by ligand exchange of surface hydroxyl groups and formation of surface complexes.
- Detachment of surface metal species, usually facilitated by polarization of metal-oxygen bonds within the mineral structure.
- Regeneration of the surface site and transport of the detached metal into bulk solution.

Because the detachment of surface complexes is usually the rate-limiting step, rate laws of surface-controlled reaction can be derived in terms of the concentration of surface complexes (Duckworth et al., 2009b; Martin, 2005; Stumm, 1997)

Surface complexes formed from adsorption reactions can affect metal to lattice bond strength by donating electron density, thus weakening the critical metal-oxygen bonds. The rate of dissolution is proportional to the surface concentration of a precursor complex:

$$R_L = k_L [ > Me - L ] \quad (1)$$

where  $R_L$  is the dissolution rate,  $k_L$  is the corresponding dissolution rate coefficient, and  $[ > Me - L ]$  is the concentration of active surface complexes. Any factors that influence the ligand surface concentration or coordination are also likely to influence dissolution rates. Bidentate

ligands such as hydroxamates can form relatively strong bidentate surface complexes that have a significantly greater effect on oxide dissolution kinetics than monodentate surface complexes (Stumm, 1987). Even among bidentate surface complexes, five-membered chelate rings tend to have a higher effect on dissolution rates than six- or seven-membered rings (Duckworth and Martin, 2001; Furrer and Stumm, 1986).

#### *1.5.4 Reductive Dissolution*

Reductive dissolution involves electron transfer between ligands and surface metal, which is a surface-controlled process. Adsorption reactions produce inner-sphere and outer-sphere surface complexes, both of which may be precursors to electron transfer reactions. Electron transfer via the inner-sphere mechanism is limited by ligand exchange rates of surface metal centers whereas an outer-sphere mechanism results in reactions that are independent of ligand exchange rates (Martin, 2005; Stone and Marsalek, 1996). The electron transfer causes reduction of surface metal with the concomitant oxidation of the ligand. The bond between the surface metal and the lattice oxygen is weakened by reduction so that detachment of metals is favored. As with ligand-promoted non reductive dissolution, detachment of the metal ion is often the rate determining step in reductive dissolution (Stone and Morgan, 1984).

#### *1.5.5 Proton Promoted Dissolution*

Mineral dissolution may also occur via a proton-promoted pathway that is distinct from ligand-promoted and reductive dissolution reactions. The protonation of surface sites polarizes the critical bonds between metal centers and lattice, promoting the dissolution of metal oxides.

The fast adsorption of protons onto the surface is followed by a slow detachment of the metal ion from crystal lattice, which is the rate-limiting step. Because the protonated surface sites are precursors of the rate-determining step, a rate law can be expressed as a function of surface excess of adsorbed protons ( $[H]_{ads}$ )

$$R_H = k_H [H]_{ads}^n \quad (2)$$

where  $k_H$  is dissolution rate constant, and  $n$  as reaction order.  $[H]_{ads}$  can be related to the concentration of the protonated surface sites (Stone and Ulrich, 1989). The exponent ( $n$ ) is approximately equal to the charge on the dissolving metal (Furrer and Stumm, 1986; Stone and Ulrich, 1989). Except at extreme pH, proton-promoted dissolution is the slowest of the different type of dissolution for common transition metal oxides and hydroxides (Martin, 2005).

## **1.6 Siderophore-Promoted Dissolution Minerals**

### *1.6.1 Iron Minerals*

Siderophores promote Fe dissolution from a wide range of minerals including lepidocrite, ferrihydrite, and hornblende (Liermann et al., 2000; Watteau and Berthelin, 1994). DFOB-promoted dissolution of iron hydroxides such as goethite occurs via a pH-independent, ligand-promoted (non-reductive) process that occurs on the surface of the mineral (Cocozza et al., 2002; Hersman et al., 1995). Dissolution is initiated by the formation of an inner sphere complex through direct bonding between a hydroxamate functional group in the siderophore

and an iron atom in the mineral surface (Cocozza et al., 2002; Holmén and Casey, 1996; Holmén et al., 1997). In the absence of light at pH = 6, hydrolysis of the terminal hydroxamate group of DFOB at the Fe-hydroxide surface may produce decomposition products of acetate and an oxidized hydroxylamine-DFOB fragment, which could indicate the reduction of Fe(III) to Fe(II), suggesting both a reductive and ligand-promoted pathway for goethite dissolution (Simanova et al., 2010).

### *1.6.2 DFOB-Promoted Dissolution of Metal Oxides*

The stability constants of siderophores with trivalent transition metals can approach or exceed those with Fe(III). These relatively high stability constants, together with the common occurrence of siderophores in metal rich soil and aqueous environments suggest that siderophores could potentially have impacts on the transport and mobility of trace and other metals. DFOB-promoted dissolution of FeOOH has been extensively studied and shown to proceed by a largely pH independent and non-reductive process (Cheah et al., 2003; Cocozza et al., 2002; Hersman et al., 1995; Reichard et al., 2005; Reichard et al., 2007; Wolff-Boenisch and Traina, 2007; Yoshida et al., 2002). However, recent studies shows that DFOB dissolves CoOOH and MnOOH via a reductive pathway at pH < 7 and a ligand-promoted pathway at pH > 7 (Bi et al., 2010; Duckworth et al., 2009b; Duckworth and Sposito, 2005a). Because the dissolution rate and mechanism likely depends on the type of siderophore as well as the metal hydroxide, this thesis will utilize representative siderophore structures (Figure 1.1) to estimate the range of siderophore reactivity in the environment as a way to understand their different mechanisms of dissolution.

### *1.6.3 Siderophore-Promoted Mineral Dissolution in the Presence of Low Molecular Mass*

#### *Organic Acids*

Siderophores are not produced in isolation by microbes and plants, but are co-exuded with other low molecular mass organic acids, such as citrate and oxalate (Cheah et al., 2003; Reichard et al., 2007). The secretion of these low molecular mass acids is known to be part of a strategy to promote mineral solubility and increase their bioavailability. Low molecular mass organic acids can behave like catalysts by using their moieties to speed up the exchange of Fe(III) at the surface of the goethite structure (Cheah et al., 2003). For example, in the presence of DFOB, Fe(III)-oxalate complex detachment from the surface is favored (Loring et al., 2007), and Fe is removed from the oxalate complex by ligand exchange because of DFOB's higher affinity for Fe(III).

Once deferrated, these low molecular mass organic acids are free to complex other Fe(III) ions on the surface of the goethite (like a molecular shuttle (Reichard et al., 2007)) whereas the Fe(III)-siderophore complex is available for cellular uptake. By acting in this way, there is a combined effect where the low molecular mass organic ligands aid in the transport of Fe from the goethite surface to the siderophores, and in doing so, increase the dissolution rate more than in the presence of either component alone (Cheah et al., 2003; Reichard et al., 2007). A similar observation was made with MnO<sub>2</sub> in the presence of DFOB and low molecular mass organic acids (Saal and Duckworth, 2010). To date, little information about the synergistic effect on dissolution goethite rates by low molecular mass organic acids with siderophores other than DFOB and phytosiderophores. This thesis will explore possible

synergistic effects on dissolution of goethite as promoted by oxalate and the siderophores used in this study.

## **1.7 Summary**

Trace metals, such as Fe, Mn, and Co, are essential in minute quantities for the well-being of most living things. However, at elevated concentrations, such as found in polluted and contaminated sites, they may be highly toxic and, when released into aquifers, surface waters, sediments, or soils via human activities, can enter the food chain via example uptake by microbial cells or plant roots. In natural systems, siderophores have been implicated in the mobilization of heavy metals and radionuclide into the environment in alkaline soils (Edberg et al., 2010; Kalinowski et al., 2006; Xu and Raymond, 2006). It is therefore very important to gain a deeper understanding of the fate of trace metals in the environment, and the various interactions and role that these organic ligands play in the environment in the cycling of these metals. Despite the amount of growing awareness of the diverse environmental chemistry of siderophores, there is still limited knowledge and understanding of how siderophores and siderophore-containing multi-ligand mixtures solubilize trace metals from their oxides, and of surface interactions between metal-siderophore complexes with other metal oxides at environmentally relevant aqueous conditions (Duckworth et al., 2009a; Kraemer, 2004). This knowledge is critical for understanding the role of siderophores in biological metal uptake, the cycling of trace metals, and in the fate and transport of metals in soils and natural waters. The objectives of this thesis are to

- To determine the dissolution rate and mechanisms of trivalent Fe, Mn, and Co hydroxides in the presence of DFOB, protochelin, and rhizoferrin, siderophores that are representative of broad classes of these ligands
- To determine the co-effects of small molecular mass complexing organic acids on the dissolution rates of goethite as promoted by DFOB, protochelin, and rhizoferrin.

## 1.8 References

1. Adriano, D.C., 2001. Trace elements in terrestrial environments: biogeochemistry, bioavailability, and risks of metals. Springer, New York.
2. Albrecht-Gary, A.M., Crumbliss, A.L., 1998. Coordination chemistry of siderophores: Thermodynamics and kinetics of iron chelation and release. Iron transport and storage in microorganisms, plants, and animals 35, 239-327.
3. Anderegg, G.v., l'Eplattenier, F., Schwarzenbach, G., 1963. Hydroxamatkomplexe II. Die Anwendung der pH-Methode. Helvetica Chimica Acta 46, 1400-1408.
4. Bartlett, R.J., 1988. Manganese redox reactions and organic interactions in soils, Manganese in soils and plants. Springer, pp. 59-73.
5. Batinic-Haberle, I., Birus, M., Pribanic, M., 1991. Siderophore chemistry of vanadium. Kinetics and equilibrium of interaction between vanadium (IV) and desferrioxamine B in aqueous acidic solutions. Inorganic chemistry 30, 4882-4887.
6. Baysse, C., De Vos, D., Naudet, Y., Vandermonde, A., Ochsner, U., Meyer, J.-M., Budzikiewicz, H., Schäfer, M., Fuchs, R., Cornelis, P., 2000. Vanadium interferes with siderophore-mediated iron uptake in *Pseudomonas aeruginosa*. Microbiology 146, 2425-2434.
7. Bellenger, J.P., Wichard, T., Kustka, A.B., Kraepiel, A.M.L., 2008. Uptake of molybdenum and vanadium by a nitrogen-fixing soil bacterium using siderophores. Nature Geoscience 1, 243-246.
8. Bi, Y., Hesterberg, D.L., Duckworth, O.W., 2010. Siderophore-promoted dissolution of cobalt from hydroxide minerals. Geochimica et Cosmochimica Acta 74, 2915-2925.
9. Bondietti, G., Sinniger, J., Stumm, W., 1993. The reactivity of Fe (III)(hydr) oxides: effects of ligands in inhibiting the dissolution. Colloids and Surfaces A: Physicochemical and Engineering Aspects 79, 157-167.
10. Borch, T., Kretzschmar, R., Kappler, A., Cappellen, P.V., Ginder-Vogel, M., Voegelin, A., Campbell, K., 2009. Biogeochemical redox processes and their impact on contaminant dynamics. Environmental science & technology 44, 15-23.
11. Boukhalfa, H., Crumbliss, A.L., 2002. Chemical aspects of siderophore mediated iron transport. Biometals 15, 325-339.

12. Brown Jr, G.E., Henrich, V., Casey, W., Clark, D., Eggleston, C., Felmy, A., Goodman, D.W., Gratzel, M., Maciel, G., McCarthy, M.I., 1999. Metal oxide surfaces and their interactions with aqueous solutions and microbial organisms *Chem. Rev.* 99, 77–174.
13. Cheah, S.F., Kraemer, S.M., Cervini-Silva, J., Sposito, G., 2003. Steady-state dissolution kinetics of goethite in the presence of desferrioxamine B and oxalate ligands: implications for the microbial acquisition of iron. *Chemical Geology* 198, 63-75.
14. Coccozza, C., Tsao, C.C.G., Cheah, S.F., Kraemer, S.M., Raymond, K.N., Miano, T.M., Sposito, G., 2002. Temperature dependence of goethite dissolution promoted by trihydroxamate siderophores. *Geochimica et Cosmochimica Acta* 66, 431-438.
15. Cornell, R.M., Schwertmann, U., 2003. *The iron oxides: structure, properties, reactions, occurrences and uses.* Weinheim, Wiley-VCH, 2003
16. Dahlheimer, S.R., Neal, C.R., Fein, J.B., 2007. Potential mobilization of platinum-group elements by siderophores in surface environments. *Environmental science & technology* 41, 870-875.
17. Dosanjh, N.S., Michel, S.L., 2006. Microbial nickel metalloregulation: NikRs for nickel ions. *Current opinion in chemical biology* 10, 123-130.
18. Drever, J.I., 1997. *The Geochemistry of Natural Waters: Surface and Groundwater Environments.* Prentice Hall, Upper Saddle River, NJ 7458, 436.
19. Duckworth, O., Bargar, J., Sposito, G., 2009a. Coupled biogeochemical cycling of iron and manganese as mediated by microbial siderophores. *Biometals* 22, 605-613.
20. Duckworth, O.W., Bargar, J.R., Jarzecki, A.A., Oyerinde, O., Spiro, T.G., Sposito, G., 2009b. The exceptionally stable cobalt(III)–desferrioxamine B complex. *Marine Chemistry* 113, 114-122.
21. Duckworth, O.W., Holmström, S.J.M., Peña, J., Sposito, G., 2009c. Biogeochemistry of iron oxidation in a circumneutral freshwater habitat. *Chemical Geology* 260, 149-158.
22. Duckworth, O.W., Martin, S.T., 2001. Surface complexation and dissolution of hematite by C1 to C6 dicarboxylic acids at pH= 5.0. *Geochimica et Cosmochimica Acta* 65, 4289-4301.

23. Duckworth, O.W., Sposito, G., 2005a. Siderophore-manganese (III) interactions II. Manganite dissolution promoted by desferrioxamine B. *Environmental science & technology* 39, 6045-6051.
24. Duckworth, O.W., Sposito, G., 2005b. Siderophore-manganese (III) interactions. I. Air-oxidation of manganese (II) promoted by desferrioxamine B. *Environmental science & technology* 39, 6037-6044.
25. Duhme, A.-K., Dauter, Z., Hider, R.C., Pohl, S., 1996. Complexation of molybdenum by siderophores: Synthesis and structure of the double-helical cis-dioxomolybdenum (VI) complex of a bis (catecholamide) siderophore analogue. *Inorganic chemistry* 35, 3059-3061.
26. Dzombak, D.A., Morel, F.M., 1990. *Surface complexation modeling: hydrous ferric oxide*. Wiley New York.
27. Edberg, F., Kalinowski, B.E., Holmström, S.J.M., Holm, K., 2010. Mobilization of metals from uranium mine waste: the role of pyoverdines produced by *Pseudomonas fluorescens*. *Geobiology* 8, 278-292.
28. Evers, A., Hancock, R.D., Martell, A.E., Motekaitis, R.J., 1989. Metal ion recognition in ligands with negatively charged oxygen donor groups. Complexation of iron (III), gallium (III), indium (III), aluminum (III), and other highly charged metal ions. *Inorganic chemistry* 28, 2189-2195.
29. Farkas, E., Szabo, O., 2012. Co (II) and Co (III) hydroxamate systems: A solution equilibrium study. *Inorganica chimica acta* 392, 354-361.
30. Furrer, G., Stumm, W., 1986. The coordination chemistry of weathering: I. Dissolution kinetics of  $\delta$ -Al<sub>2</sub>O<sub>3</sub> and BeO. *Geochimica et Cosmochimica Acta* 50, 1847-1860.
31. Garibaldi, J., Neilands, J., 1956. Formation of iron-binding compounds by microorganisms *Nature* 177, 526 - 527.
32. Ghose, S.K., Waychunas, G.A., Eng, P.J., Trainor, T.P., 2008. Structure and reactivity of hydrated goethite (100) interface and Arsenic sorption: CTR and RAXR study. *Geochimica et Cosmochimica Acta Supplement* 72, 307.
33. Graham, R.D., Hannam, R.J., Uren, N.C., 1988. *Manganese in soils and plants*. Kluwer Academic Publishers, 261-276.

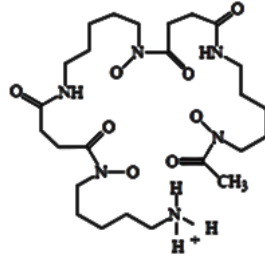
34. Harrington, J.M., Parker, D.L., Bargar, J.R., Jarzecki, A.A., Tebo, B.M., Sposito, G., Duckworth, O.W., 2012. Structural dependence of Mn complexation by siderophores: Donor group dependence on complex stability and reactivity. *Geochimica et Cosmochimica Acta* 88, 106-119.
35. Hernlem, B.J., Vane, L.M., Sayles, G.D., 1996. Stability constants for complexes of the siderophore desferrioxamine B with selected heavy metal cations. *Inorganica chimica acta* 244, 179-184.
36. Hersman, L., Lloyd, T., Sposito, G., 1995. Siderophore-promoted dissolution of hematite. *Geochimica et Cosmochimica Acta* 59, 3327-3330.
37. Hider, R.C., Kong, X., 2010. Chemistry and biology of siderophores. *Nat. Prod. Rep.* 27, 637-657.
38. Holmén, B.A., Casey, W.H., 1996. Hydroxamate ligands, surface chemistry, and the mechanism of ligand-promoted dissolution of goethite  $\alpha$ -FeOOH(s). *Geochimica et Cosmochimica Acta* 60, 4403-4416.
39. Holmén, B.A., Tejedor-Tejedor, M.I., Casey, W.H., 1997. Hydroxamate complexes in solution and at the goethite-water interface: A cylindrical internal reflection Fourier transform infrared spectroscopy study. *Langmuir* 13, 2197-2206.
40. Holmström, M., Kallio, E., 2004. The solar wind interaction with Venus and Mars: energetic neutral atom and X-ray imaging. *Advances in Space Research* 33, 187-193.
41. Jarvis, N.V., Hancock, R.D., 1991. Some correlations involving the stability of complexes of transuranium metal ions and ligands with negatively charged oxygen donors. *Inorganica chimica acta* 182, 229-232.
42. Kalinowski, B., Johnsson, A., Arlinger, J., Pedersen, K., Odegaard-Jensen, A., Edberg, F., 2006. Microbial mobilization of uranium from shale mine waste. *Geomicrobiology Journal* 23, 157-164.
43. Kim, D., Duckworth, O.W., Strathmann, T.J., 2009. Hydroxamate siderophore-promoted reactions between iron(II) and nitroaromatic groundwater contaminants. *Geochimica et Cosmochimica Acta* 73, 1297-1311.
44. Kraemer, S.M., 2004. Iron oxide dissolution and solubility in the presence of siderophores. *Aquatic Sciences-Research Across Boundaries* 66, 3-18.
45. Kraemer, U., 2003. Phytoremediation to phytochelatin – plant trace metal homeostasis. *New Phytologist* 158, 1469-8137.

46. Kraepiel, A., Bellenger, J., Wichard, T., Morel, F., 2009. Multiple roles of siderophores in free-living nitrogen-fixing bacteria. *Biometals* 22, 573-581.
47. Kruft, B.I., Harrington, J.M., Duckworth, O.W., Jarzecki, A.A., 2013. Quantum mechanical investigation of aqueous desferrioxamine B metal complexes: Trends in structure, binding, and spectroscopy. *Journal of Inorganic Biochemistry*.
48. Li, Y., Zamble, D.B., 2009. Nickel homeostasis and nickel regulation: an overview. *Chemical reviews* 109, 4617-4643.
49. Liermann, L.J., Kalinowski, B.E., Brantley, S.L., Ferry, J.G., 2000. Role of bacterial siderophores in dissolution of hornblende. *Geochimica et Cosmochimica Acta* 64, 587-602.
50. Loper, J.E., Buyer, J.S., 1991. Siderophores in microbial interactions on plant surfaces. *Mol. Plant-Microbe Interact* 4, 5-13.
51. Loring, J.S., Simanova, A.A., Persson, P., 2007. Molecular scale study of the synergism between oxalate and desferrioxamine-B on goethite dissolution, *Geochimica et Cosmochimica Acta*, pp. A596-A596.
52. Lund, T.J., Koretsky, C.M., Landry, C.J., Schaller, M.S., Das, S., 2008. Surface complexation modeling of Cu (II) adsorption on mixtures of hydrous ferric oxide and kaolinite. *Geochemical transactions* 9, 9.
53. Martin, S.T., 2005. Precipitation and dissolution of iron and manganese oxides. *Environmental Catalysis*, 61-81.
54. McArdell, C.S., Stone, A.T., Tian, J., 1998. Reaction of EDTA and related aminocarboxylate chelating agents with CoOOH (heterogenite) and MnOOH (manganite). *Environmental science & technology* 32, 2923-2930.
55. Mucha, R.F., Geier, A., Pauli, P., 1999. Modulation of craving by cues having differential overlap with pharmacological effect: evidence for cue approach in smokers and social drinkers, *Psychopharmacology* 147 (1999), pp. 306-313. *Psychopharmacology* 147, 306-313.
56. Parker, D.L., Sposito, G., Tebo, B.M., 2004. Manganese(III) binding to a pyoverdine siderophore produced by a manganese(II)-oxidizing bacterium. *Geochimica et Cosmochimica Acta* 68, 4809-4820.

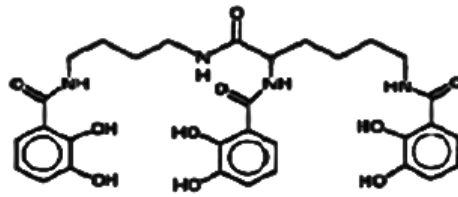
57. Penn, R.L., Stone, A.T., Veblen, D.R., 2001. Defects and disorder: Probing the surface chemistry of heterogenite (CoOOH) by dissolution using hydroquinone and iminodiacetic acid. *The Journal of Physical Chemistry B* 105, 4690-4697.
58. Post, J.E., 1999. Manganese oxide minerals: Crystal structures and economic and environmental significance. *Proceedings of the National Academy of Sciences* 96, 3447-3454.
59. Raymond, N.K., 1994. Recognition and transport of natural and synthetic siderophores by microbes. *Pure & Appl. Chem.*, 66, 773-781.
60. Reichard, P.U., Kraemer, S.M., Frazier, S.W., Kretzschmar, R., 2005. Goethite dissolution in the presence of phytosiderophores: rates, mechanisms, and the synergistic effect of oxalate. *Plant and soil* 276, 115-132.
61. Reichard, P.U., Kretzschmar, R., Kraemer, S.M., 2007. Dissolution mechanisms of goethite in the presence of siderophores and organic acids. *Geochimica et Cosmochimica Acta* 71, 5635-5650.
62. Römheld, V., Marschner, H., 1981. Iron deficiency stress induced morphological and physiological changes in root tips of sunflower. *Physiologia Plantarum* 53, 354-360.
63. Saal, L.B., Duckworth, O.W., 2010. Synergistic dissolution of manganese oxides as promoted by siderophores and small organic acids. *Soil Science Society of America Journal* 2010 74, 2021-2031.
64. Schaller, M.S., Koretsky, C.M., Lund, T.J., Landry, C.J., 2009. Surface complexation modeling of Cd (II) adsorption on mixtures of hydrous ferric oxide, quartz and kaolinite. *Journal of Colloid and Interface Science* 339, 302-309.
65. Schwab, A., Lindsay, W., 1983. The effect of redox on the solubility and availability of manganese in a calcareous soil. *Soil Science Society of America Journal* 47, 217-220.
66. Schwertmann, U., Cornell, R.M., 1991. Iron oxides in the laboratory : preparation and characterization. VCH, Weinheim ; New York.
67. Schwertmann, U., Taylor, R., 1989. Iron oxides. Pp. 379-438 in: *Minerals in Soil Environments* (JB Dixon and SB Weed, editors). Soil Science Society of America, Madison, Wisconsin, USA.

68. Silva, J.R.R.F., Williams, R.J.P., 1991. The biological chemistry of the elements : the inorganic chemistry of life. Clarendon Press; Oxford University Press, Oxford England New York.
69. Simanova, A.A., Persson, P., Loring, J.S., 2010. Evidence for ligand hydrolysis and Fe (III) reduction in the dissolution of goethite by desferrioxamine-B. *Geochimica et Cosmochimica Acta* 74, 6706-6720.
70. Sparks, D.L., 2001. Elucidating the fundamental chemistry of soils: past and recent achievements and future frontiers. *Geoderma* 100, 303-319.
71. Stone, A.T., Morgan, J.J., 1984. Reduction and dissolution of manganese (III) and manganese (IV) oxides by organics: 2. Survey of the reactivity of organics. *Environmental science & technology* 18, 617-624.
72. Stone, A.T., Ulrich, H.-J., 1989. Kinetics and reaction stoichiometry in the reductive dissolution of manganese (IV) dioxide and Co (III) oxide by hydroquinone. *Journal of Colloid and Interface Science* 132, 509-522.
73. Stone, M., Marsalek, J., 1996. Trace metal composition and speciation in street sediment: Sault Ste. Marie, Canada. *Water, Air, and Soil Pollution* 87, 149-169.
74. Stumm, W., 1987. *Aquatic surface chemistry: Chemical processes at the particle-water interface*. Wiley Interscience, New York.
75. Stumm, W., 1997. Reactivity at the mineral-water interface: dissolution and inhibition. *Colloids and Surfaces A: Physicochemical and Engineering Aspects* 120, 143-166.
76. Stumm, W., Morgan, J.J., 1996. *Aquatic chemistry, chemical equilibria and rates in natural waters*. Wiley Interscience, New York.
77. Sverjensky, D.A., Sahai, N., 1996. Theoretical prediction of single-site surface-protonation equilibrium constants for oxides and silicates in water. *Geochimica et Cosmochimica Acta* 60, 3773-3797.
78. Tebo, B.M., Johnson, H.A., McCarthy, J.K., Templeton, A.S., 2005. Geomicrobiology of manganese (II) oxidation. *Trends in Microbiology* 13, 421-428.
79. Twort, F., Ingram, G., 1912. A Method for Isolating and Cultivating the *Mycobacterium enteritidis chronicae pseudotuberculosis bovis*, Johne, and some Experiments on the Preparation of a Diagnostic Vaccine for Pseudo-tuberculous Enteritis of Bovines. *Proceedings of the Royal Society of London. Series B, Containing Papers of a Biological Character* 84, 517-542.

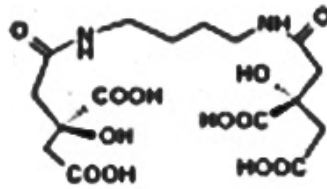
80. Vraspir, J.M., Butler, Alison, 2009. Chemistry of Marine Ligands and Siderophores. *Annu. Rev. Mar. Sci.* 1, 43-63.
81. Watteau, F., Berthelin, J., 1994. Microbial dissolution of iron and aluminium from soil minerals: efficiency and specificity of hydroxamate siderophores compared to aliphatic acids. *European Journal of Soil Biology* 30, 1-9.
82. Whisenhunt, D.W., Neu, M.P., Hou, Z., Xu, J., Hoffman, D.C., Raymond, K.N., 1996. Specific sequestering agents for the actinides. 29. Stability of the thorium (IV) complexes of desferrioxamine B (DFO) and three octadentate catecholate or hydroxypyridinonate DFO derivatives: DFOMTA, DFOCAMC, and DFO-1, 2-HOPO. Comparative stability of the plutonium (IV) DFOMTA complex. *Inorganic chemistry* 35, 4128-4136.
83. Winkelmann, G., 2002. Microbial siderophore-mediated transport. *Biochemical Society Transactions* 30, 691.
84. Wolff-Boenisch, D., Traina, S.J., 2007. The effect of desferrioxamine B on the desorption of U (VI) from Georgia kaolinite KGa-1b and its ligand-promoted dissolution at pH 6 and 25 C. *Chemical Geology* 242, 278-287.
85. Xu, J., Raymond, K.N., 2006. Structurally Characterized Quadruple Stranded Bisbidentate Helicates. *Angewandte Chemie* 118, 6630-6635.
86. Yoshida, T., Hayashi, K.-i., Ohmoto, H., 2002. Dissolution of iron hydroxides by marine bacterial siderophore. *Chemical Geology* 184, 1-9.



DFOB



Protochelin



Rhizoferrin

Figure 1.1. Molecular structure of plant and bacterial siderophores showing structural diversity and functional groups

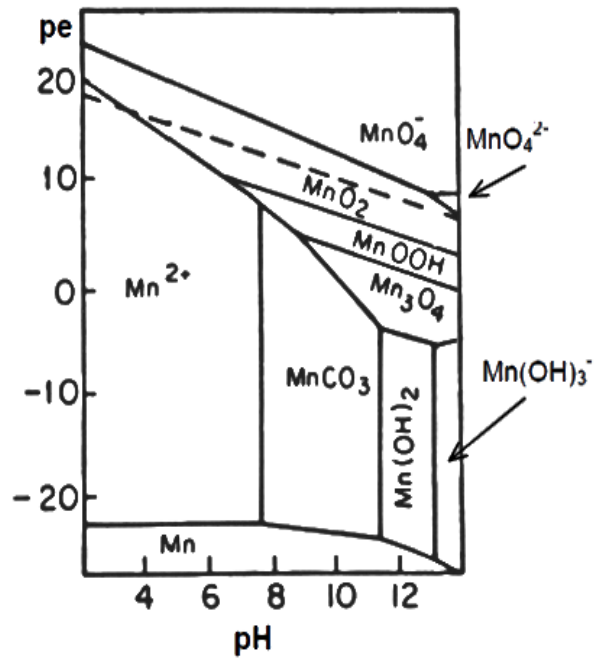


Figure 1.2. Predominance diagram Showing Mn speciation different pH and Eh conditions. Figure is reproduced from (Stumm and Morgan, 1996).

Table 1.1 Stability constants of metal-HDFOB complexes.

<b>Ion (M<sup>n+</sup>)</b>	<b>LogK<sub>MHDFOB</sub><sup>n-2</sup></b>	<b>Reference</b>
Al <sup>3+</sup>	25.5	Evers et al. (1989)
Ca <sup>2+</sup>	3.5	Anderegg et al. (1963)
Cd <sup>2+</sup>	8.8	Anderegg et al. (1963)
Co <sup>2+</sup>	10.1	Duckworth et al. (2009)
Co <sup>3+</sup>	37.4	Duckworth et al. (2009)
Cu <sup>2+</sup>	14.6	Hernlem et al. (1996)
Cu <sup>2+</sup>	14.4	Hernlem et al. (1996)
Cu <sup>2+</sup>	15.0	Anderegg et al. (1963)
Fe <sup>2+</sup>	11.1	Kim et al. (2009)
Fe <sup>3+</sup>	31.9	Anderegg et al. (1963)
Ga <sup>3+</sup>	29.5	Evers et al. (1989)
In <sup>3+</sup>	21.9	Evers et al. (1989)
La <sup>3+</sup>	12.2	Anderegg et al. (1963)
Mg <sup>2+</sup>	5.2	Anderegg et al. (1963)
Mn <sup>2+</sup>	7.7	Duckworth et al. (2005)
Mn <sup>3+</sup>	29.9	Duckworth et al. (2005)
Ni <sup>2+</sup>	11.8	Anderegg et al. (1963)
Pb <sup>2+</sup>	10.9	Hernlem et al. (1996)
Pu <sup>4+</sup>	32.6	Jarvis and Hancock (1991)
Sn <sup>2+</sup>	22.0	Hernlem et al. (1996)
Th <sup>4+</sup>	28.4	Whisenhunt et al. (1996)
Yb <sup>3+</sup>	17.3	Anderegg et al. (1963)
Zn <sup>2+</sup>	10.4	Hernlem et al. (1996)
Zn <sup>2+</sup>	12.0	Anderegg et al. (1963)
Sr <sup>2+</sup>	3.1	Anderegg et al. (1963)
Pd <sup>2+</sup>	19.2-23.2	Dahlheimer et al. (2007)
Pt <sup>2+</sup>	16.2-17.2	Dahlheimer et al. (2007)

## **Chapter 2**

### **Siderophore Promoted Dissolution of FeOOH, MnOOH, and CoOOH in the Presence and Absence of Oxalate**

## 2.1 Introduction

All microbes require trace metal nutrients, such as Co, Mn, Fe, for energy generation and proper metabolic function (Da Silva and Williams, 1991; Todar, 2009). The mineralogy and speciation of these metals are complicated, with environmental and edaphic factors, including pH, redox state, and presence of organic matter, dictating the predominant form found in soils. Under oxic conditions at circumneutral pH, these metals tend to be locked in insoluble hydroxide and primary minerals that are not readily available for biological uptake (Adriano, 2001). To overcome the potential limits on organism nutrition caused by low bioavailability of iron and possibly other metals, bacteria and fungi exude organic molecules, such as low molecular mass organic acids and siderophores, to promote mineral dissolution and increase metal solubility (Bagg and Neilands, 1987).

Siderophores (derived from Greek meaning “iron carrier”) are specialized chelating agents exuded by microorganisms during iron stress to enhance iron availability. The effectiveness of siderophores comes from their ability to form soluble complexes with iron that have high stability constants, making the iron biologically available for uptake by microbes. Currently, about 500 different types of siderophores have been discovered (Hider and Kong, 2010). These biomolecules are structurally diverse, but typically are tetra- or hexa-dentate ligands with oxygen bearing moieties that directly bind a central metal ion (viz. Fe(III)) (Crumbliss and Harrington, 2009). Although most geochemical studies have utilized the trihydroxamate siderophore desferrioxamine B (DFOB), it is reasonable to assume that they may display a range of reactivity, largely dictated by the nature of the ligand moieties that interact directly with the metal center.

An important role of siderophores in soils is thought to be promoting the dissolution of iron from poorly soluble minerals. Desferrioxamine B has been shown to promote iron dissolution from a number of different phases, including oxides, hydroxides, phosphates, sulfides, and clay minerals (Cervini-Silva et al., 2012; Cervini-Silva and Sposito, 2002; Cornejo-Garrido et al., 2008; Haack et al., 2008; Liermann et al., 2005; Liermann et al., 2000; Rosenberg and Maurice, 2003; Wolff-Boenisch and Traina, 2007). The DFOB-promoted dissolution of FeOOH has been shown to proceed by a surface controlled mechanism, resulting in the formation of a Fe(III)HDFOB<sup>+</sup> complex (Cheah et al., 2003). Interestingly, in the presence of siderophores and low molecular mass organic acids (such as oxalate), the dissolution rate of goethite is enhanced beyond a simple addition of the single-component dissolution rates (Cervini-Silva and Sposito, 2002; Cheah et al., 2003; Wolff-Boenisch and Traina, 2007). This “synergistic” effect results from oxalate acting as an iron shuttle that delivers iron Fe(III) to dissolved siderophores, possibly with detachment of the oxalate surface complexes favored by the presence of the siderophore (Loring et al., 2007).

Despite the assumed high specificity of siderophores for ferric iron, strong interactions between DFOB and other metals have been recognized for over 50 years (Anderegg et al., 1963). More recent studies have shown that siderophores may promote the uptake of metals other than Fe(III), including Mo and V (Anderegg et al., 1963; Budzikiewicz et al., 2002; Duhme-Klair, 2009; Kraepiel et al., 2009b). Metals such as Mn(III) and Co(III) may have stability constants with siderophores that rival or exceed those of Fe (Duckworth et al., 2009a; Duckworth et al., 2009b; Duckworth et al., 2008a, b; Duckworth et al., 2009c; Duckworth and Martin, 2001; Duckworth and Sposito, 2005a; Duckworth and Sposito, 2005b; Harrington and

Crumbliss, 2009; Parker et al., 2004). Furthermore, DFOB promotes the dissolution of both MnOOH and CoOOH at rates that exceed those of FeOOH by several orders magnitude. Interestingly, these minerals dissolve by a reductive pathway (producing divalent metals) at low pH whereas they produce complexes via ligand promoted dissolution under alkaline conditions.

Although the interactions between DFOB and iron-bearing minerals have been well studied, little information exists probing the mechanisms of dissolution of Fe(III) hydroxide by other siderophores (Cervini-Silva, 2008; Wolff-Boenisch and Traina, 2007), a fact that limits our understanding of the function of siderophores in soil and natural waters (Kraemer, 2004). In addition, there have been few studies probing the interactions of siderophores other than DFOB with Mn and Co minerals. In this chapter, I will quantify and compare the dissolution rates of FeOOH, MnOOH, and CoOOH as promoted by several different structurally diverse microbial siderophores in the absence and presence of oxalic acid. In addition, I will compare their dissolution rates with the stability constants of the corresponding metal-siderophore complexes obtained to further elucidate their mechanism of dissolution.

## **2.2 Materials and Methods**

### *2.2.1 Reagents*

All solutions, acids, and calibration standards were prepared in deionized water that was purified to  $\geq 18$  m $\Omega$  prior to use. To maintain a constant pH for each experiment over the pH range of 5 to 9, 10 mM buffer solutions of acetate (Ac), 2-(*N*-morpholino)ethanesulfonic acid (MES) and 4-(2-hydroxyethyl)-1-piperazineethanesulfonic acid (HEPES) (Arcos

Organic), were utilized for pH 5, 6, and 7-9, respectively. These buffers have previously been shown not to affect DFOB-promoted dissolution of metal hydroxide (Bi et al., 2010; Duckworth and Sposito, 2005a; Duckworth and Sposito, 2005b; Saal and Duckworth, 2010).

### 2.2.2 Siderophores

The three siderophores examined in this study were chosen for their structural diversity (Figure 2.1). The mesylate salt of desferrioxamine B [DFOB;  $C_{25}H_{46}N_5O_8NH_3^+(CH_3SO_3)^-$ ], a trihydroxamate siderophore produced by several species of *Streptomyces* and *Nocardia*, (Winkelmann, 1992), was purchased from Sigma Aldrich and used without any further purification. Rhizoferrin is a carboxylate-bearing siderophore produced by the fungus *Rhizopus arrhizus* and the bacterium *Ralstonia picketti*. Our sample is a racemic mixture of both naturally occurring enantiomers (Drechsel et al., 1992; Münzinger et al., 1999). Protochelin is a naturally occurring triscatecholamide siderophore produced by the nitrogen fixing bacterium *Azotobacter vinelandii*. Both rhizoferrin and protochelin were synthesized by the Duke University Small Molecules Custom Synthesis Facility.

### 2.2.3 Synthesis of metal hydroxides

The metal hydroxides that were used in this study were synthesized via laboratory methods. Goethite ( $\alpha$ -FeOOH) was synthesized by using an established method (Schwertmann and Cornell, 1991; Schwertmann and Cornell, 2000) by precipitating 1 M  $Fe(NO_3)_3$  solution with 5 M KOH solution in a 1 L Erlenmeyer flask. After ageing for 6 hours, the mixture was centrifuged and washed with DI water five times. The solution was filtered and the solid

residue lyophilized until dry (ca. 48 hrs.). The dry solid was disaggregated with a mortar and pestle and stored in a freezer until use.

Manganite ( $\gamma$ -MnOOH) was synthesized according to literature methods (Duckworth and Sposito, 2005a; Giovanoli, 1969; McArdell et al., 1998). Solutions of 0.2 M  $\text{NH}_4\text{OH}$ , 0.06 M  $\text{MnSO}_4$ , and 30%  $\text{H}_2\text{O}_2$  were each purged for 1 h with  $\text{N}_2$ . A 1 L solution of  $\text{MnSO}_4$  solution was stirred continuously in a 2 L Erlenmeyer flask. 20.4 mL solution of  $\text{N}_2$ -purged 30%  $\text{H}_2\text{O}_2$  was added to the  $\text{MnSO}_4$  solution. After stirring for 15 minutes, 300 mL of  $\text{N}_2$ -purged  $\text{NH}_4\text{OH}$  solution was slowly added to the 2 L flask with vigorous stirring, resulting in the formation of a dark-brown precipitate. The suspension was rapidly heated to the boiling point, and then maintained at 98 °C under reflux with constant stirring for 6 h. The resulting mixture was then filtered while hot and washed with 500 mL of hot DI water during filtration. The residue was then cold-washed by suspension and sonication in deionized water for 15 min, followed by centrifugation for 15 min at 15000 rpm speed. The washing process was repeated five times. The washed solid was then freeze dried for 48 hours, after which the solid was disaggregated with a mortar and pestle, and stored in a freezer until use. The heterogenite is the same sample used by Bi et al. (2010), and its synthesis and properties previously have been described.

#### *2.2.4 Particle characterization*

Dried Fe and Mn hydroxide minerals were characterized to determine morphology, phase, and specific surface area. Samples for Transmission Electron Microscopy (TEM) analysis were prepared by dispersing solid particles in methanol. A drop of suspension was placed onto the surface of 3 mm carbon filmed Cu grid. After allowing the suspension to dry

for 2 min, TEM micrographs of synthesized solid were collected on a Hitachi HF-2000. TEM for both FeOOH and MnOOH samples showed particles with uniform needle-like shape with an average length of approximately 700 nm and 300-500 nm respectively (Appendix Figures A2.1-A2.2). Powder X-ray diffraction (XRD) patterns of solid samples were collected from 15-95° 2 $\theta$  with an Intel XRG-3000 Diffractometer equipped with a Co-K $\alpha$  source ( $\lambda = 1.789$  Å). This confirmed the mineral phase of synthesized solids as goethite and manganite (Appendix). Brunauer–Emmett–Teller (BET) surface area analyses of the three minerals determined by nitrogen adsorption using an Autosorb-1-MP surface pore analyzer (Quantachrome Corp.) measured 69 and 48.9 g m<sup>-2</sup> for COOH and MnOOH. Bi et al. (2010) reported a BET surface area of 59.8 g m<sup>-2</sup> for the CoOOH used in this study.

#### *2.2.5 Siderophore-promoted dissolution of goethite, heterogenite, and manganite*

Dissolution rates and products of metal hydroxides were investigated as a function of pH from 5-9 both in the absence and presence of siderophores. Batch experiments were utilized to conserve limited quantities of siderophore. A 150 mL solution of 0.1 M NaCl electrolyte solution with 10 mM buffer was prepared in 250 mL Erlenmeyer flask. An aliquot (50 mL) was pipetted from the 150 ml solution of buffer and electrolyte into a 50 mL conical flask to which a proscribed mass of siderophore was added. Next, 0.03 g of metal hydroxide was added to the remaining 100 mL of the buffer and electrolyte solution in the 250 mL Erlenmeyer flask and sonicated for about 15 min to disperse particles.

The flask was then wrapped with an aluminum foil and placed into a temperature controlled water bath maintained at 25°C. The contents of the flask were mixed with a Teflon

stir bar and a magnetic stir plates placed under the water bath and covered to prevent the interference of light but not to exclude oxygen. After allowing the reaction temperature to equilibrate, the 50 mL buffer and electrolyte and siderophore solution were then added to the 100 mL solution in the 250 mL reaction container in the bath and quickly covered with aluminum foil to prevent light from interfering with the experiment.

For FeOOH, a 2 mL aliquot was quickly drawn out using a syringe and immediately filtered using a 0.2  $\mu\text{m}$  filter. Subsequent 2 mL aliquots were taken at 12 hour intervals over a 14 day period. For MnOOH, the 2 mL aliquots were taken at 0, 2.5, 5, 7.5, 10, 15, 20, 30, 45 and 60 minutes intervals, whereas samples for CoOOH were collected at 15 minute intervals up to three hours. At each pH, three replicates were conducted for experiments for DFOB and two replicates for both protochelin and rhizoferrin. Control experiments were conducted in duplicate in the absence of siderophore.

#### *2.2.6 Dissolution of goethite, heterogenite and manganite in the presence of oxalate and siderophores*

The dissolution rates of metal hydroxide by siderophores in the presence of oxalate were conducted as batch experiments in 250 mL Erlenmeyer flasks wrapped with aluminum foil to prevent exposure to light. Stock solutions of 0.0017 M DFOB, 0.0036 M rhizoferrin, 0.0048 M protochelin and 0.216 M oxalate were prepared in 25 mL and 10 mL flasks just prior to the start of the experiments. A 150 mL solution of 0.1 M NaCl electrolyte solution was prepared to which a 10 mM buffer was added. Metal hydroxide (0.03 g) was added to the 150 mL solution with the buffer in the electrolyte solution in the 250 mL Erlenmeyer flask and

sonicated for 15 minutes. The flask was then wrapped with an aluminum foil and placed into a temperature controlled water bath maintained at 25°C. The contents of the flask was kept stirring by a magnetic stirrer and a magnetic stir plates placed under the water bath. After allowing the reaction temperature to equilibrate, the 150 mL buffer and electrolyte solution was spiked with 0.638 mL of the 0.216 M oxalate solution, resulting in a total concentration of 1 mM. For FeOOH–oxalate solution, 2 mL aliquots were collected at the following times; 0, 24, 48, 72 and 96 hours.

The remaining mineral suspension was spiked with siderophore stock solution (3.85 mL DFOB, 3.75 mL rhizoferrin, or 2.85 mL protochelin) to produce a total concentration of 100  $\mu$ M in the remaining solution for each experiment. Following siderophore addition, 2 mL aliquots were collected at 8 hour intervals for up to 12 days. For the MnOOH-oxalate experiment, initial 2 mL aliquots were collected at 0, 5, 10, 15, 20, 25 and 30 minutes before spiking with the same amount of siderophore stock solution as in the FeOOH experiments to result in a 100  $\mu$ M siderophore concentration in the remaining solution, after which 2 mL aliquots were taken at 5 min intervals up to 1 h. For CoOOH-oxalate experiment, 2 mL aliquots were taken at 15 min intervals up to an hour before addition of the same amount of siderophore to stock solution as for the FeOOH experiments described earlier; after siderophore addition, aliquots were collected at 15 minute intervals for up to 3 h. All aliquots were immediately filtered with 0.2 micron filters and supernatant stored for analysis. Two replicates were conducted for each experimental condition and experimental control reactions were replicated similarly with oxalate in the absence of siderophores.

### *2.2.7 Quantification of dissolved siderophore complexes*

The pH of each aliquot taken was measured with a Fisher Scientific XL 25 pH meter with a glass electrode. The siderophore-metal complex concentration was measured immediately after sampling by pouring 1 mL of sample into a 1 cm cuvette. The sample was then analyzed using the Ocean optics UV-visible spectrometer to measure sample concentration using wavelength and a Beer-Lambert extinction coefficient obtained from literature (Table 2.1). The 1 mL sample was added back to the original aliquot and stored in the dark at 4°C prior to total dissolved metal analysis. Because of the potentially shorter temporal stability of Mn and Co siderophore complexes (Harrington et al., 2012), UV-visible spectral measurements for these samples were taken within an hour after the completion of experiments for all the runs. Quantification of the more stable Fe(III)-complexes was conducted on a daily basis after sampling.

### *2.2.8 Atomic absorption spectrometry*

The samples were acidified with trace metal grade HCl and diluted ca. 7-30 times to bring sample concentrations within linear range of the Thermo-Fisher flame atomic absorption spectrometer (FAAS). For pH = 5-6 for CoOOH and MnOOH, 0.2 mL of sample was added to 1 mL of trace metal grade HCl and diluted to 6.2 mL with DI water. For pH = 7-9 for these metals as well as FeOOH at all pH, 1 mL of sample was added to 1 mL of trace metal grade HCL and diluted to 7 ml with DI water. Total dissolved metal concentration was quantified by FAAS to determine trends in metal concentration as a function of time.

### 2.2.9 Quantification of dissolution rates

In the presence of siderophores and the absence of oxalate, dissolution of metal hydroxides may proceed by proton-promoted ( $R_H$ ), ligand-promoted ( $R_L$ ), or reductive pathways ( $R_R$ ), all of which may occur simultaneously. As such, the total dissolution rate ( $R_T$ ) is the sum the rate of dissolution from each pathway:

$$R_T = R_H + R_R + R_L \quad (1)$$

Control experiments conducted in the absence of siderophore show that the proton promoted dissolution rates for MnOOH, CoOOH, and FeOOH were negligible at all pH values. Hence, dissolution is assumed to occur only by reduction of the metal ion center without the formation of a metal-siderophore complex (reductive dissolution) and by formation of a complex where the oxidation state of the metal center is retained (ligand promoted dissolution):



where reductive dissolution results in concomitant oxidation of some part of the siderophore.

For all experiments, plots of both metal-siderophore complex (in the presence and absence of oxalate) and total metal dissolution were initially linear and approached a maximum value towards the end of the reaction (Figures 2.2- 2.3). To calculate initial dissolution rates, linear regression analysis was performed on the first 7-10 points, resulting in with an  $R^2$  value

between 0.91 and 0.98; the overall dissolution rates were then calculated and tested at 95% confident interval, which was used to estimate error. The total dissolution rate ( $R_{Sox}$ ) of the metal hydroxides by siderophores in the presence of oxalic acid were also calculated and tested at 95% confident interval by performing linear regression analysis on the first 3-5 linear points after siderophore addition. The  $R^2$  value varied between 0.90 and 0.98 for these regressions.

## 2.3 Results and Discussion

### 2.3.1 Trends in Siderophore-promoted Dissolution Rates for Metal Oxide.

The siderophore-promoted total dissolution rates of FeOOH, MnOOH, and CoOOH as promoted by DFOB, rhizoferrin, and protochelin are shown in Figure 2.4. Generally, the dissolution rate decreased with increasing pH for MnOOH and CoOOH with all three siderophores. FeOOH dissolution was pH independent for DFOB and rhizoferrin but increased with pH for protochelin. The total dissolution rates of CoOOH and MnOOH at all pH were generally faster than for FeOOH (Figure 2.9). Protochelin-promoted dissolution rates for each mineral were faster than DFOB and rhizoferrin at all pH, with the exception of FeOOH at pH = 5. Interestingly, protochelin-promoted and DFOB-promoted dissolution rates for MnOOH and CoOOH were within error of each other. Dissolution rates for MnOOH as promoted by rhizoferrin at all pH were faster than those for CoOOH and FeOOH.

Dissolution rates for different minerals promoted by the same reaction pathway often trend with the water exchange rates (Casey and Ludwig, 1996; Westrich et al., 1993). Previous work by Nowack and Sigg (1996) and McArdel et al. (1998) showed that ligand promoted dissolution rates of CoOOH by ethylenediaminetetraacetic acid (EDTA) and nitrilotriacetic

acid (NTA) were lower than those for FeOOH and MnOOH. Both NTA and EDTA have the same carboxylic functional group found in rhizoferrin. However, from the above, results we see that the dissolution rates of MnOOH, CoOOH, and FeOOH by the siderophores do not follow the order predicted from the waters of exchange of these metals (Helm and Merbach, 1999; Morgan, 2000), which would be in the order MnOOH > FeOOH > CoOOH. This lack of a trend has been previously observed for DFOB (Bi et al., 2010), who noted the same reaction order observed in this study, and is supported by results with the other siderophores utilized in this study.

### *2.3.2 Siderophore-promoted dissolution of FeOOH.*

Figure 2.5 shows the initial siderophore-promoted dissolution rate of FeOOH at 25 °C in 0.1 M NaCl electrolyte solution. In all cases, total dissolved metal concentration did not exceed the concentration of siderophore (100 µM) added, and Fe(III)-siderophore complexes were detected photometrically at all pH. For DFOB and rhizoferrin, the total dissolution rates are within error of the ligand-promoted dissolution rates, indicating a predominantly ligand promoted dissolution pathway. DFOB-promoted dissolution rates follow the pH-dependent trends reported in the literature (Cervini-Silva, 2008; Coccozza et al., 2002; Kraemer et al., 1999; Lloyd, 1999; Wolff-Boenisch and Traina, 2007). However, the rates measured in this study are an order of magnitude faster than reported surface area normalized dissolution rates, which vary from  $7.32 \times 10^{-13}$  to  $2.5 \times 10^{-12}$  mol m<sup>-2</sup> s<sup>-1</sup> for DFOB-promoted dissolution of FeOOH (cf. Table 2.2). Although it is not completely clear why the rates in this study are faster than previously reported, the rates reported in this work are initial dissolution rates derived

from batch experiments whereas most literature rates are steady-state rates derived from continuous flow experiments.

The initial dissolution rates may reflect contributions from high-energy sites (MacInnis and Brantley, 1992), and commonly exceed steady-state dissolution rates (Duckworth and Sposito, 2005a; Kraemer, 2004). When compared to initial DFOB-promoted FeOOH dissolution rates derived from batch experiments, our rates are approximately one order of magnitude faster literature rates (Carrano et al., 1996; Lloyd, 1999; Neubauer et al., 2002; Wolff-Boenisch and Traina, 2007) for almost the same amount of DFOB used (Table 2.3). We do not have an explanation for this discrepancy between our dissolution rates and those in the literature, although difference in experimental conditions (solids loading, ionic strength, concentration, etc.) may account for some variation in rates.

The FeOOH dissolution rates as promoted by DFOB and rhizoferrin are largely pH-independent. This could possibly be because the speciation of both DFOB and rhizoferrin does not change over the pH range of the experiments. For DFOB, the sorption to FeOOH surfaces and dissolution rates have previously been shown to be largely pH independent (Carrano et al., 1996). Although no such sorption data exists to aid in our interpretation for rhizoferrin, (Lindgren et al., 2009) used Fourier transform infrared spectroscopy to show that the sorption of citrate, an  $\alpha$ -hydroxycarboxylate that is similar in structure to rhizoferrin, is largely invariant in concentration and dominated by single surface complex for  $4 \leq \text{pH} \leq 7$ , consistent with a pH-invariant ligand-promoted dissolution rate observed for rhizoferrin. For protochelin, calculated ligand-promoted dissolution rates are less than total rates at  $\text{pH} \leq 7$ , and exceed total rates at  $\text{pH} \geq 8$ . Because ligand promoted rates cannot exceed total dissolution rates and we do

not anticipate other types of dissolution reactions to occur at  $\text{pH} \leq 7$ , we believe the discrepancy between ligand promoted and total dissolution rates to be derived from partial degradation of protochelin, which results in a colored complex that may interfere with photometric quantification of the complex (Harrington et al., 2012). The rate of protochelin-promoted dissolution increases with increasing pH. It should be noted that protochelin, undergoes a speciation change near  $\text{pH} = 7$ , protochelin is deprotonated at  $\text{pH} > 7$  and fully protonated at  $\text{pH} \leq 7$ . This may help to explain the observed pH-dependent trends in dissolution rate. Overall, our results at  $\text{pH} = 6$  agree well with FeOOH initial dissolution rates promoted by enterobactin, a structurally similar catecholate siderophore (Wolff-Boenisch and Traina, 2007).

Dissolution rates may trend with the stabilities of aqueous complexes. The stability constant of the Fe(III)Protochelin<sup>3-</sup> complex is  $10^{44.6}$  (Dubme et al., 1997), which is higher than the stability constants for Fe(III)HDFOB<sup>+</sup> ( $10^{32.0}$ ) and Fe(III)Rhizoferrin<sup>3-</sup> ( $10^{25.3}$ ) (Anderegg et al., 1963; Carrano et al., 1996). It has previously been reported that dissolution rates trend with stability constants for a group of structurally homologous DFOB derivatives (Cervini-Silva and Sposito, 2002). A plot (Figure 2.6) showing a compilation of initial dissolution rates for FeOOH derived from batch reactors as promoted by different siderophores from our study and the literature (Table 2.3) shows a positive correlation ( $p > 0.05$ ) with the log stability constants of the ligand to Fe. The trend implies that, if the activated complex at the mineral surface is similar to the metal-organic acid complex in solution (Furrer and Stumm, 1986) and the rate determining step in the dissolution of metal hydroxides is the detachment of the metal-ligand complex from the structure of the metal, the ligand-promoted dissolution rate of FeOOH can be predicted from the ligand-metal stability constant (Ludwig et al., 1995).

### 2.3.3 Siderophore-promoted dissolution of CoOOH and MnOOH

Siderophore-promoted dissolution rates are shown for CoOOH and MnOOH as a function of pH in Figures 2.7-2.8 and Tables 2.4- 2.5. Dissolution rates generally follow a pH dependent trend with decreasing dissolution rate as pH increased for all siderophores. The rates for protochelin exceed those of DFOB and rhizoferrin, with difference most pronounced at low pH. For MnOOH, total dissolution rates trended with Mn(III)-complex stability constants, as for FeOOH (Figure 2.6); for CoOOH, there is currently insufficient data to generate an equivalent plot. In all cases except DFOB-promoted dissolution at alkaline pH (for MnOOH,  $\text{pH} \geq 7$ ; for CoOOH,  $\text{pH} \geq 8$ ), dissolution occurs exclusively by a reductive pathway. In situations where complexes were detected, ligand-promoted and total dissolution rates were within error of one another, suggesting a predominantly ligand-promoted dissolution pathway. Dissolution rates at pH values where reductive dissolution was dominant had dissolved metal concentrations that exceeded siderophore concentrations by 3 to 12 times, suggesting that the siderophore can react multiple times with the surface. For DFOB, pH-dependent trends in dissolution rates, and numerical dissolution rates agree well with those of previous workers, who reported dissolution rates of  $1.2 \times 10^{-10}$  to  $2.5 \times 10^{-10} \text{ mol m}^{-2} \text{ s}^{-1}$  for MnOOH (Duckworth and Sposito, 2005a) and for CoOOH (Bi et al., 2010) with rates between  $0.5 \times 10^{-10}$  and  $2.7 \times 10^{-9} \text{ mol m}^{-2} \text{ s}^{-1}$  for  $\text{pH} = 5-9$ .

Only reductive dissolution is observed for protochelin- and rhizoferrin-promoted dissolution of CoOOH and MnOOH. Previous work has shown that Co(III)-protochelin complexes are unstable at all pH, and Mn(III)-protochelin complexes are only transiently stable at alkaline pH (Harrington and Crumbliss, 2009). It is thus not surprising that protochelin

dissolved both CoOOH and MnOOH solely by reductive pathways. It is more surprising that rhizoferrin only undergoes reductive dissolution with MnOOH and CoOOH. Rhizoferrin has been shown to form a stable complex with Mn(III) at alkaline pH. Although previous reports of attempts to form Co(III)-rhizoferrin complexes were unsuccessful (Carrano et al., 1996), a Co(III)-rhizoferrin complex that was synthesized by oxidation of Co(II) with H<sub>2</sub>O<sub>2</sub> was spectroscopically confirmed to be Co(III) (Appendix A2.6; Table A2.1). In addition, citrate, which is an  $\alpha$ -hydroxycarboxylate that is structurally related to rhizoferrin, has been shown to promote dissolution by reductive dissolution at pH  $\leq 6$  (Klewicki and Morgan, 1999). However, at pH  $\geq 7$ , a high concentration of the ligand promotes dissolution by both a reductive and non-reductive process, forming an initial unstable Mn(III)-citrate complex which disintegrates by internal electron transfer after 10 to 20 hours to form Mn(II) products (Klewicki and Morgan, 1998). It is possible that an excess concentration of rhizoferrin with our experiment could have produced metal-siderophore complexes at high pH, although we did not test this hypothesis.

The Mn(II) and Co(II) that are formed during reductive dissolution may form complexes with siderophores, but these complexes are of lower affinity than the trivalent metals. This trend can be explained by noting that the hard Lewis base donor groups bind more favorably with the hard Lewis acid trivalent ions. For DFOB, where the largest database of stability constants exists, the trivalent metal stability constants ( $\log K_{Co(III)HDFOB} = 37.4$  and  $\log K_{Mn(III)HDFOB} = 29.9$ ) exceed those of divalent by  $> 20$  orders of magnitude ( $\log K_{Co(II)HDFOB} = 10.1$  and  $\log K_{Mn(II)HDFOB} = 7.7$ ) (Anderegg et al., 1963; Duckworth et al., 2009b; Duckworth and Sposito, 2005a). The association between the siderophores and these divalent cations are

weak, and a large fraction of siderophore may be free to react with the surface. In addition, it has been proposed that siderophores may undergo multiple redox reactions with surfaces, resulting in degradation of the siderophore (Duckworth and Sposito, 2005a; Duckworth and Sposito, 2005b; Duckworth and Sposito, 2007).

#### *2.3.4 Siderophore-promoted dissolution rates of metal hydroxides in the presence of oxalate.*

The dissolution rates of FeOOH in the presence of oxalate and siderophores are shown in Figures 2.10-2.12 and Table 2.6-2.7. Previous work has shown that in the presence of oxalate and DFOB at pH = 5-6, the dissolution rate for FeOOH is approximately 2-fold greater than the sum of the dissolution rates of individual components. Our results at slightly different experimental condition, which show a 3-fold enhancement of the sum of total DFOB- and oxalate- promoted dissolution rates at corresponding conditions, are consistent with these literature reports (Cheah et al., 2003; Reichard et al., 2007). In the presence of oxalate, dissolution of FeOOH by protochelin is greatly enhanced as compared to sum of dissolution rate of each ligand in the system, with dissolution increasing 9-fold at pH = 6; a three-fold enhancement is observed at pH = 8. However, oxalate had an inhibitory effect on rhizoferrin-promoted dissolution at pH = 6, with rate equaling rate in the presence of oxalate alone. At pH = 8, dissolution rates for DFOB and rhizoferrin are within error of the sum of oxalate and siderophore promoted rates in the absence of DFOB, indicating a lack of a synergistic effect on dissolution.

The synergistic effects of oxalate on siderophore-promoted dissolution result from oxalate acting as an iron shuttle that delivers iron Fe(III) to dissolved siderophores, possibly

with detachment of the oxalate surface complexes favored by the presence of the siderophore (Loring et al., 2007). This conceptual model may be used to help interpret our results. The extent to which the dissolution rate is promoted depends on the solution pH as well as the stability constant of the iron-siderophore complex. The pH of the system determines the surface charge on the mineral surface as well as the charge and the protonation state of the oxalate moieties. At pH = 6, dissolution rates trend with the stability constant of the siderophore. The log stability constant of the trisoxalto-Fe(III) complex is 30.75 (Mollar et al., 1991). Although this stability constant is > 10 orders of magnitude lower than that of protochelin, it is similar in magnitude to that of DFOB and exceeds that of rhizoferrin. This suggests that at high concentration of oxalate, trisoxalto-Fe(III) complexes may persist in solution containing DFOB (as noted by Cheah et al. (2003) in UV-visible measurements), slowing the synergistic process. In addition, it suggest that it is not thermodynamically favorable for rhizoferrin to remove Fe(III) from tris-oxalato complexes, explaining the lack of a synergistic promotion of rates in the presence of rhizoferrin and oxalate. At pH = 8, the sorption of oxalate onto FeOOH has been shown to be very weak, with only low surface concentrations obtained (Eick et al., 1999; Mesuere and Fish, 1992), consistent with the lack an effect on the dissolution rates of FeOOH by DFOB and rhizoferrin, and marked reduction of its effect on the dissolution rate of protochelin.

As compared to FeOOH, oxalate had a smaller impact on the siderophore-promoted CoOOH and MnOOH dissolution rates (Table 2.6). Protochelin increased dissolution rates by approximately a factor of two at pH = 6 for MnOOH and CoOOH at pH = 8; however, no increase in rate was observed for MnOOH at pH = 8, and there was no increase in rate for

CoOOH at pH = 6. Similarly, DFOB and rhizoferrin did not have enhanced dissolution rates in the presence of oxalate as compared to the sum of the one-ligand systems. This result is somewhat surprising because Saal and Duckworth (2010) noted a 2-3 fold increase in reductive dissolution rates for MnO<sub>2</sub> in the presence of oxalate, although they were unable to determine a specific mechanism. Differences in mineral phases could also account for the difference in the dissolution rates.

## 2.4 Summary and Conclusion

This chapter reported the dissolution of three metal hydroxides, CoOOH, FeOOH, and MnOOH, as promoted by DFOB, rhizoferrin, and protochelin in the presence and absence of oxalate. In general, siderophore-promoted dissolution rates followed the order MnOOH > CoOOH > FeOOH (Figure 2.9). Protochelin produced the largest dissolution rates for all three metal hydroxides. For FeOOH, dissolution rates increased with increasing pH; for CoOOH and MnOOH, rates increased with decreasing pH. Rhizoferrin and DFOB promoted dissolution of MnOOH and CoOOH were same order of magnitude and was pH dependent decreasing with increasing pH. These results extend prior results obtained with DFOB to siderophores comprised of differing functional groups, filling a significant knowledge gap in the literature.

For FeOOH, dissolution by all three siderophores occurred via a predominantly ligand-promoted pathway. Protochelin-promoted dissolution rates increased with increasing pH, and exceeded those of the other siderophores except a pH = 5. DFOB promoted dissolution rates were larger than for rhizoferrin, with both siderophores exhibiting pH independent

dissolution rates. By incorporating dissolution rates with a literature data set at pH = 6, the logarithm of siderophore promoted dissolution rates are shown to correlate with the logarithm of stability constants, extending a previous result derived for a small set of DFOB-derivatives. In contrast to results with FeOOH, reductive dissolution was dominant for MnOOH and CoOOH at all pH for rhizoferrin and protochelin and at pH  $\leq$  8 for CoOOH and at pH  $\leq$  7 for MnOOH for DFOB. This clearly work shows the reactivity of organic ligands with metal hydroxides depend on their functional groups and that under similar environmental conditions, they may react differently with the metal hydroxides in the environment.

Siderophores are not produced in isolation but often in concert with low molecular mass organic acids. The presence of oxalate may enhance, inhibit, or have no effect on siderophore -promoted dissolution rates. At pH = 6, the difference in measured stability constants between the organic acid and the siderophore may dictate whether siderophore have a synergistic effect on dissolution. At pH = 8, oxalate sorption to minerals is reduced and thus their effect on siderophore-promoted dissolution is reduced. The synergistic effect was particularly pronounced for protochelin, which increased FeOOH dissolution rates 3- to 9-fold as compared to single ligand system. Because protochelin is prone to degradation at environmental relevant pH values (Harrington et al., 2012), the use of oxalate may be an important part of a protochelin-based uptake system.

## 2.5 References

1. Adriano, D.C., 2001. Trace elements in terrestrial environments: biogeochemistry, bioavailability, and risks of metals. Springer, New York.
2. Anderegg, G., l'Eplattenier, F., Schwarzenbach, G., 1963. Hydroxamatkomplexe II. Die Anwendung der pH-Methode. *Helvetica Chimica Acta* 46, 1400-1408.
3. Bagg, A., Neilands, J., 1987. Ferric uptake regulation protein acts as a repressor, employing iron (II) as a cofactor to bind the operator of an iron transport operon in *Escherichia coli*. *Biochemistry* 26, 5471-5477.
4. Bi, Y., Hesterberg, D.L., Duckworth, O.W., 2010. Siderophore-promoted dissolution of cobalt from hydroxide minerals. *Geochimica et Cosmochimica Acta* 74, 2915-2925.
5. Budzikiewicz, H., Georgias, H., Taraz, K., 2002. Diastereomeric pyoverdinin-chromium (III) complexes. *Zeitschrift für Naturforschung C* 57, 954-956.
6. Carrano, C.J., Drechsel, H., Kaiser, D., Jung, G., Matzanke, B., Winkelmann, G., Rochel, N., Albrecht-Gary, A.M., 1996. Coordination chemistry of the carboxylate type siderophore rhizoferrin: the iron (III) complex and its metal analogs. *Inorganic chemistry* 35, 6429-6436.
7. Casey, W.H., Ludwig, C., 1996. The mechanism of dissolution of oxide minerals. *Nature* 381, 506-509.
8. Cervini-Silva, J., 2008. Adsorption of Trihydroxamate and Catecholate Siderophores on  $\alpha$ -Iron (Hydr) oxides and their Dissolution at pH 3.0 to 6.0. *Soil Science Society of America Journal* 72, 1557-1562.
9. Cervini-Silva, J., Kearns, J., Banfield, J., 2012. Steady-State Dissolution Kinetics of Mineral Ferric Phosphate in the Presence of Desferrioxamine-B and Oxalate Ligands at pH= 4 to 6 and T= 24±0.6° C. *Chemical Geology* 320-321, 1-8.
10. Cervini-Silva, J., Sposito, G., 2002. Steady-state dissolution kinetics of aluminum-goethite in the presence of desferrioxamine-B and oxalate ligands. *Environmental science & technology* 36, 337-342.
11. Cheah, S.F., Kraemer, S.M., Cervini-Silva, J., Sposito, G., 2003. Steady-state dissolution kinetics of goethite in the presence of desferrioxamine B and oxalate ligands: implications for the microbial acquisition of iron. *Chemical Geology* 198, 63-75.

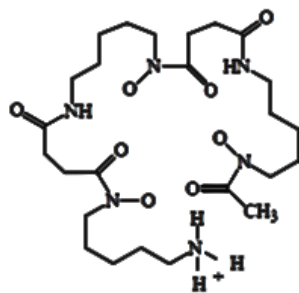
12. Coccozza, C., Tsao, C.C.G., Cheah, S.F., Kraemer, S.M., Raymond, K.N., Miano, T.M., Sposito, G., 2002. Temperature dependence of goethite dissolution promoted by trihydroxamate siderophores. *Geochimica et Cosmochimica Acta* 66, 431-438.
13. Cornejo-Garrido, H., Fernandez-Lomelan, P., Guzman, J., Cervini-Silva, J., 2008. Dissolution of arsenopyrite (FeAsS) and galena (PbS) in the presence of desferrioxamine-B at pH 5. *Geochimica et Cosmochimica Acta* 72, 2754-2766.
14. Crumbliss, A.L., Harrington, J.M., 2009. Iron sequestration by small molecules: Thermodynamic and kinetic studies of natural siderophores and synthetic model compounds. *Advances in Inorganic Chemistry* 61, 179-120.
15. Da Silva, J.F., Williams, R.J.P., 1991. *The biological chemistry of the elements : the inorganic chemistry of life*. Clarendon Press;Oxford University Press, Oxford England New York.
16. Drechsel, H., Jung, G., Winkelmann, G., 1992. Stereochemical characterization of rhizoferrin and identification of its dehydration products. *Biometals* 5, 141-148.
17. Dubme, A.K., Hider, R.C., Khodr, H.H., 1997. Synthesis and Iron Binding Properties of Protochelin, the Tris (catecholamide) Siderophore of *Azotobacter vinelandii*. *Chemische Berichte* 130, 969-973.
18. Duckworth, O., Bargar, J., Sposito, G., 2009a. Coupled biogeochemical cycling of iron and manganese as mediated by microbial siderophores. *Biometals* 22, 605-613.
19. Duckworth, O.W., Bargar, J.R., Jarzecki, A.A., Oyerinde, O., Spiro, T.G., Sposito, G., 2009b. The exceptionally stable cobalt(III)-desferrioxamine B complex. *Marine Chemistry* 113, 114-122.
20. Duckworth, O.W., Bargar, J.R., Sposito, G., 2008a. Quantitative Structure- Activity Relationships for Aqueous Metal- Siderophore Complexes. *Environmental science & technology* 43, 343-349.
21. Duckworth, O.W., Bargar, J.R., Sposito, G., 2008b. Sorption of ferric iron from ferrioxamine B to synthetic and biogenic layer type manganese oxides. *Geochimica et Cosmochimica Acta* 72, 3371-3380.
22. Duckworth, O.W., Holmström, S.J.M., Peña, J., Sposito, G., 2009c. Biogeochemistry of iron oxidation in a circumneutral freshwater habitat. *Chemical Geology* 260, 149-158.

23. Duckworth, O.W., Martin, S.T., 2001. Surface complexation and dissolution of hematite by C1 to C6 dicarboxylic acids at pH= 5.0. *Geochimica et Cosmochimica Acta* 65, 4289-4301.
24. Duckworth, O.W., Sposito, G., 2005a. Siderophore-manganese (III) interactions II. Manganite dissolution promoted by desferrioxamine B. *Environmental science & technology* 39, 6045-6051.
25. Duckworth, O.W., Sposito, G., 2005b. Siderophore-manganese (III) interactions. I. Air-oxidation of manganese (II) promoted by desferrioxamine B. *Environmental science & technology* 39, 6037-6044.
26. Duckworth, O.W., Sposito, G., 2007. Siderophore-promoted dissolution of synthetic and biogenic layer-type Mn oxides. *Chemical Geology* 242, 497-508.
27. Duhme-Klair, A.K., 2009. From Siderophores and Self-Assembly to Luminescent Sensors: The Binding of Molybdenum by Catecholamides. *European Journal of Inorganic Chemistry* 2009, 3689-3701.
28. Eick, M.J., Peak, J.D., Brady, W.D., 1999. The effect of oxyanions on the oxalate-promoted dissolution of goethite. *Soil Science Society of America Journal* 63, 1133-1141.
29. Furrer, G., Stumm, W., 1986. The coordination chemistry of weathering: I. Dissolution kinetics of  $\delta$ -Al<sub>2</sub>O<sub>3</sub> and BeO. *Geochimica et Cosmochimica Acta* 50, 1847-1860.
30. Giovanoli, R., 1969. A simplified scheme for polymorphism in the manganese dioxides. *Chimia* 23, 470-472.
31. Haack, E.A., Johnston, C.T., Maurice, P.A., 2008. Mechanisms of siderophore sorption to smectite and siderophore-enhanced release of structural Fe<sup>3+</sup>. *Geochimica et Cosmochimica Acta* 72, 3381-3397.
32. Harrington, J.M., Crumbliss, A.L., 2009. The redox hypothesis in siderophore-mediated iron uptake. *Biometals* 22, 679-689.
33. Harrington, J.M., Parker, D.L., Bargar, J.R., Jarzecki, A.A., Tebo, B.M., Sposito, G., Duckworth, O.W., 2012. Structural dependence of Mn complexation by siderophores: Donor group dependence on complex stability and reactivity. *Geochimica et Cosmochimica Acta* 88, 106-119.
34. Helm, L., Merbach, A., 1999. Water exchange on metal ions: experiments and simulations. *Coordination chemistry reviews* 187, 151-181.

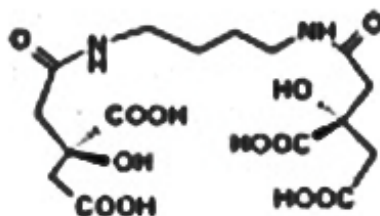
35. Hider, R.C., Kong, X., 2010. Chemistry and biology of siderophores. *Nat. Prod. Rep.* 27, 637-657.
36. Klewicki, J.K., Morgan, J.J., 1998. Kinetic behavior of Mn (III) complexes of pyrophosphate, EDTA, and citrate. *Environmental science & technology* 32, 2916-2922.
37. Klewicki, J.K., Morgan, J.J., 1999. Dissolution of  $\beta$ -MnOOH particles by ligands: pyrophosphate, ethylenediaminetetraacetate, and citrate. *Geochimica et Cosmochimica Acta* 63, 3017-3024.
38. Kraemer, S.M., 2004. Iron oxide dissolution and solubility in the presence of siderophores. *Aquatic Sciences-Research across Boundaries* 66, 3-18.
39. Kraemer, S.M., Cheah, S.-F., Zapf, R., Xu, J., Raymond, K.N., Sposito, G., 1999. Effect of hydroxamate siderophores on Fe release and Pb (II) adsorption by goethite. *Geochimica et Cosmochimica Acta* 63, 3003-3008.
40. Kraepiel, A.M.L., Bellenger, J.P., Wichard, T., Morel, F.M.M., 2009. Multiple roles of siderophores in free-living nitrogen-fixing bacteria. *Biometals* 22, 573-581.
41. Liermann, L.J., Gynn, R.L., Anbar, A., Brantley, S.L., 2005. Production of a molybdophore during metal-targeted dissolution of silicates by soil bacteria. *Chemical Geology* 220, 285-302.
42. Liermann, L.J., Kalinowski, B.E., Brantley, S.L., Ferry, J.G., 2000. Role of bacterial siderophores in dissolution of hornblende. *Geochimica et Cosmochimica Acta* 64, 587-602.
43. Lindegren, M., Loring, J.S., Persson, P., 2009. Molecular structures of citrate and tricarallylate adsorbed on  $\alpha$ -FeOOH particles in aqueous suspensions. *Langmuir* 25, 10639-10647.
44. Lloyd, T., 1999. Dissolution of Fe (III)-and Mn (III, IV)-(hydr) oxides by desferrioxamine B. California Institute of Technology: Pasadena, CA.
45. Loring, J.S., Simanova, A.A., Persson, P., 2007. Molecular scale study of the synergism between oxalate and desferrioxamine-B on goethite dissolution, *Geochimica et Cosmochimica Acta*, pp. A596-A596.
46. Ludwig, C., Casey, W.H., Rock, P.A., 1995. Prediction of ligand-promoted dissolution rates from the reactivities of aqueous complexes. *Nature* 375, 44-47.

47. MacInnis, I.N., Brantley, S.L., 1992. The role of dislocations and surface morphology in calcite dissolution. *Geochimica et Cosmochimica Acta* 56, 1113-1126.
48. McArdell, C.S., Stone, A.T., Tian, J., 1998. Reaction of EDTA and related aminocarboxylate chelating agents with CoOOH (heterogenite) and MnOOH (manganite). *Environmental science & technology* 32, 2923-2930.
49. Mesuere, K., Fish, W., 1992. Chromate and oxalate adsorption on goethite. 1. Calibration of surface complexation models. *Environmental science & technology* 26, 2357-2364.
50. Mollar, M., Castro, I., Lloret, F., Julve, M., Faus, J., Latorre, J., 1991. A solution study of complex formation between iron(III) and oxalate in dimethylsulphoxide. *Transition Met Chem* 16, 31-34.
51. Morgan, J.J., 2000. Manganese in natural waters and earth's crust: its availability to organisms. *Met Ions Biol Syst* 37, 1-34.
52. Münzinger, M., Taraz, K., Budzikiewicz, H., Drechsel, H., Heymann, P., Winkelmann, G., Meyer, J.M., 1999. S, S-rhizoferrin (enantio-rhizoferrin)—a siderophore of *Ralstonia* (*Pseudomonas*) *pickettii* DSM 6297—the optical antipode of R, R-rhizoferrin isolated from fungi. *Biometals* 12, 189-193.
53. Neubauer, U., Furrer, G., Schulin, R., 2002. Heavy metal sorption on soil minerals affected by the siderophore desferrioxamine B: the role of Fe (III)(hydr) oxides and dissolved Fe (III). *European journal of soil science* 53, 45-55.
54. Nowack, B., Sigg, L., 1996. Adsorption of EDTA and metal-EDTA complexes onto goethite. *Journal of Colloid and Interface Science* 177, 106-121.
55. Parker, D.L., Sposito, G., Tebo, B.M., 2004. Manganese(III) binding to a pyoverdinin siderophore produced by a manganese(II)-oxidizing bacterium. *Geochimica et Cosmochimica Acta* 68, 4809-4820.
56. Reichard, P.U., Kretzschmar, R., Kraemer, S.M., 2007. Dissolution mechanisms of goethite in the presence of siderophores and organic acids. *Geochimica et Cosmochimica Acta* 71, 5635-5650.
57. Rosenberg, D.R., Maurice, P.A., 2003. Siderophore adsorption to and dissolution of kaolinite at pH 3 to 7 and 22 C. *Geochimica et Cosmochimica Acta* 67, 223-229.

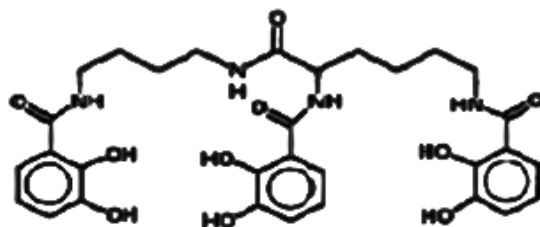
58. Saal, L.B., Duckworth, O.W., 2010. Synergistic dissolution of manganese oxides as promoted by siderophores and small organic acids. *Soil Science Society of America Journal* 2010 74, 2021-2031.
59. Schwertmann, U., Cornell, R.M., 1991. *Iron oxides in the laboratory: preparation and characterization*. VCH, Weinheim; New York.
60. Schwertmann, U., Cornell, R.M., 2000. *Iron oxides in the laboratory*. Wiley Online Library.
61. Todar, K., 2009. *The microbial world. Lectures in microbiology*. Department of Bacteriology. University of Wisconsin-Madison.
62. Westrich, H.R., Cygan, R.T., Casey, W.H., Zemitis, C., Arnold, G.W., 1993. The dissolution kinetics of mixed-cation orthosilicate minerals. *American Journal of Science* 293, 869-869.
63. Winkelmann, G., 1992. Structures and functions of fungal siderophores containing hydroxamate and complexone type iron binding ligands. *Mycological Research* 96, 529-534.
64. Wolff-Boenisch, D., Traina, S.J., 2007. The effect of desferrioxamine B on the desorption of U (VI) from Georgia kaolinite KGa-1b and its ligand-promoted dissolution at pH 6 and 25 C. *Chemical Geology* 242, 278-287.



DFOB



Protochelin



Rhizoferrin

Figure 2.1. Schematic showing the siderophores selected for use in this study. The siderophores were chosen to span the structural diversity of bacterial siderophores.

Table 2.1 Beer-Lambert extinction coefficients at specific wavelengths for metal-siderophore complexes.

Siderophore-metal complex	Beer-Lambert extinction coefficient ( $M^{-1} cm^{-1}$ )	Wavelength (nm)	Reference
FeHDFOB <sup>+</sup>	2700	425	Bi and Duckworth, 2010
MnHDFOB <sup>+</sup>	2060	310	Duckworth and Sposito, 2005
CoHDFOB <sup>+</sup>	330	425	Bi and Duckworth, 2010
FeProto <sup>3-</sup>	4600	495	Harrington et al., 2012
FeH <sub>3</sub> Proto	4600	545	Harrington et al., 2012
FeRhizo <sub>3</sub> <sup>3-</sup>	2300	335	Drechsel et al., 1992

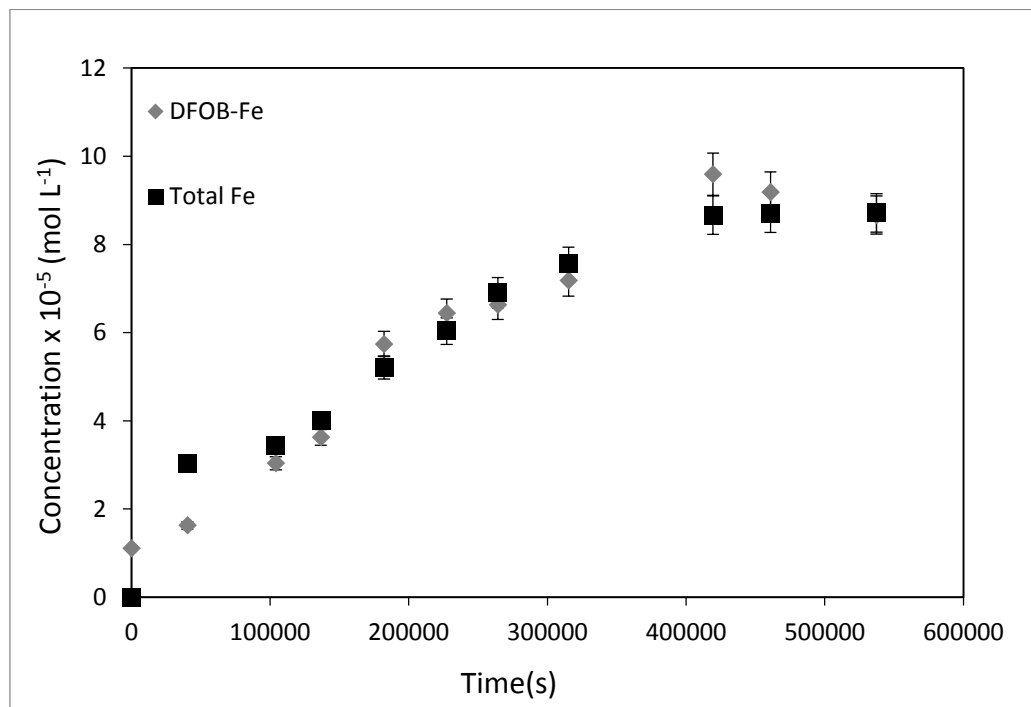


Figure 2.2. Dissolution of FeOOH as promoted by DFOB. Conditions: pH = 5; 0.2 g L<sup>-1</sup> FeOOH; 100 μM DFOB; 25°C; 10 mM acetate buffer; 0.1 M NaCl solution. Error bars present represent standard deviation of the mean.

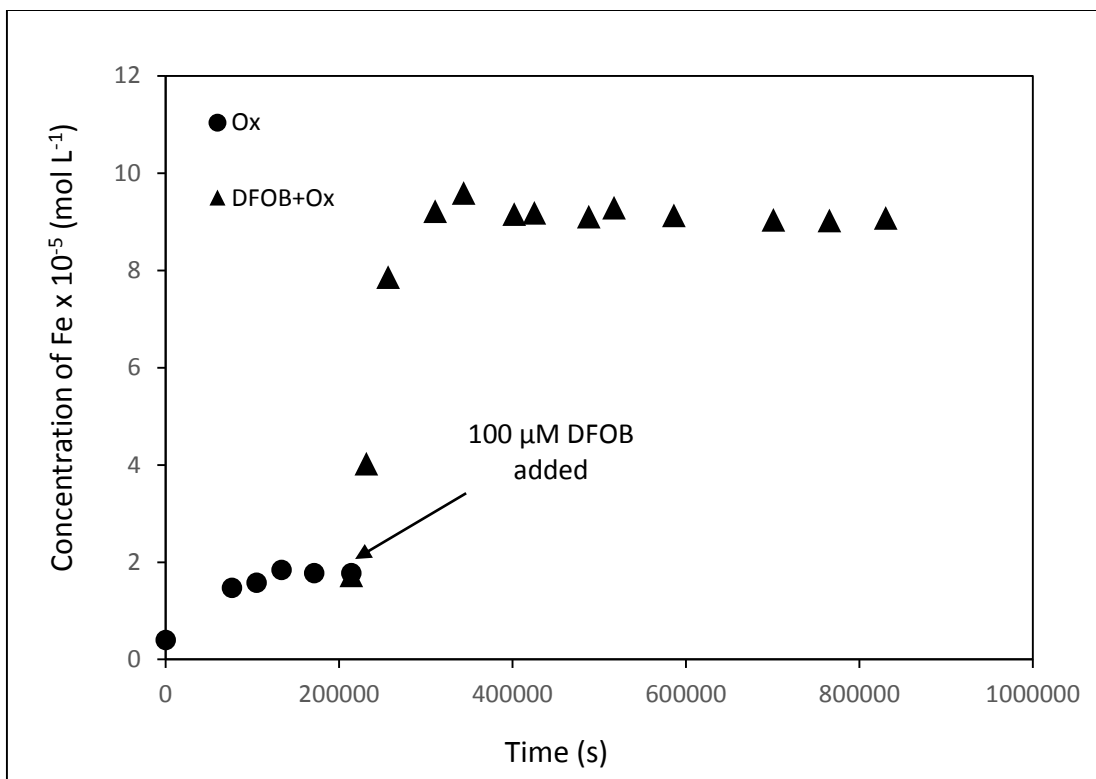


Figure 2.3. Dissolution of FeOOH as promoted by DFOB and oxalate. The experiment began with 1 mM oxalate (circles) and DFOB was added on the fourth day (triangles) Conditions: pH = 5; 0.2 g L<sup>-1</sup> FeOOH; 100 μM DFOB; 25°C; 10mM acetate buffer; 0.1 M NaCl solution.

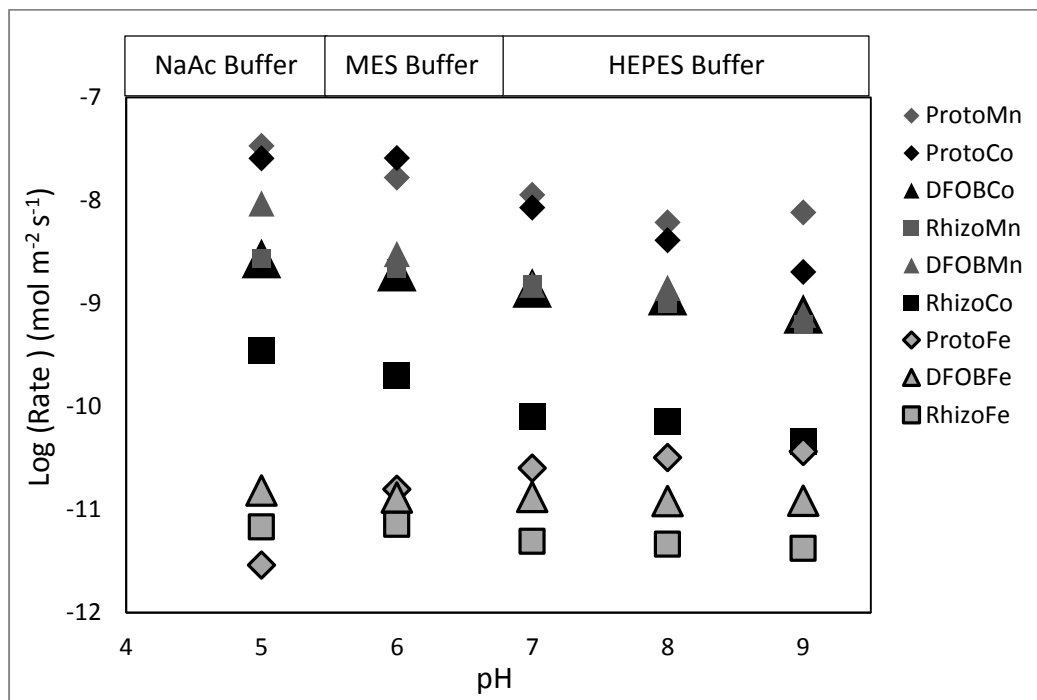


Figure 2.4. Logarithm of total initial dissolution rates coefficients for the siderophore-promoted dissolution of metal hydroxides. Conditions:  $0.2 \text{ g L}^{-1}$  MOOH;  $100 \text{ }\mu\text{M}$  siderophore;  $25^\circ\text{C}$ ;  $10 \text{ mM}$  buffer;  $0.1 \text{ M NaCl}$ . Rates are also tabulated in Table 2.2.

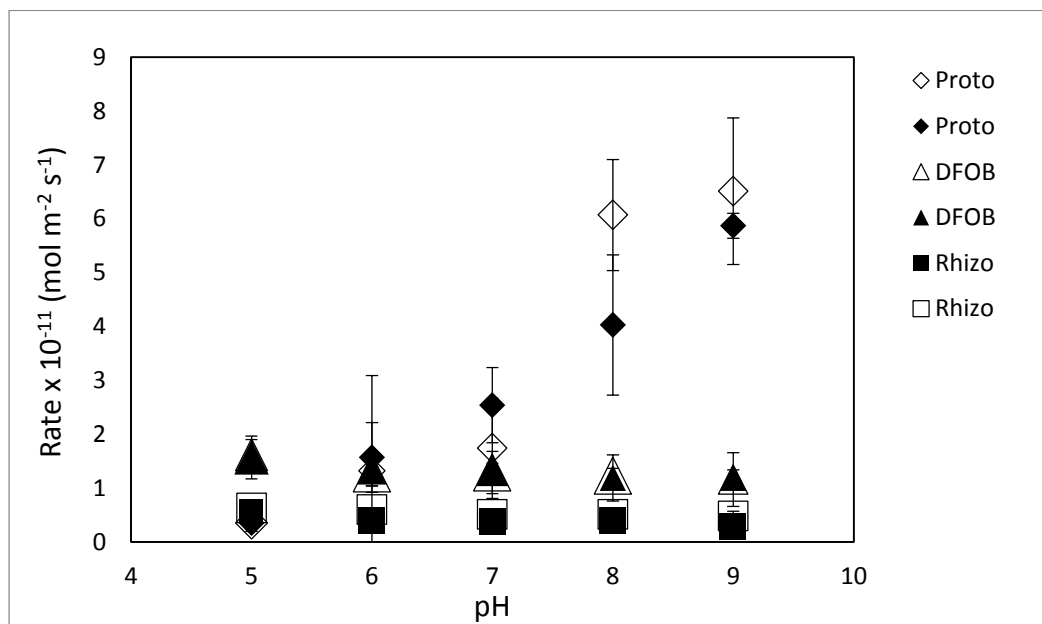


Figure 2.5. Average ligand-promoted ( $R_L$ ) (open symbol) and total ( $R_T$ ) (closed symbols) dissolution rates for FeOOH as promoted by DFOB, rhizoferrin, and protochelin. Conditions:  $0.2 \text{ g L}^{-1}$  FeOOH;  $100 \text{ }\mu\text{M}$  siderophore;  $25^\circ\text{C}$ ;  $10 \text{ mM}$  buffer;  $0.1 \text{ M}$  NaCl solution. Error bars represent 95% confidence intervals.

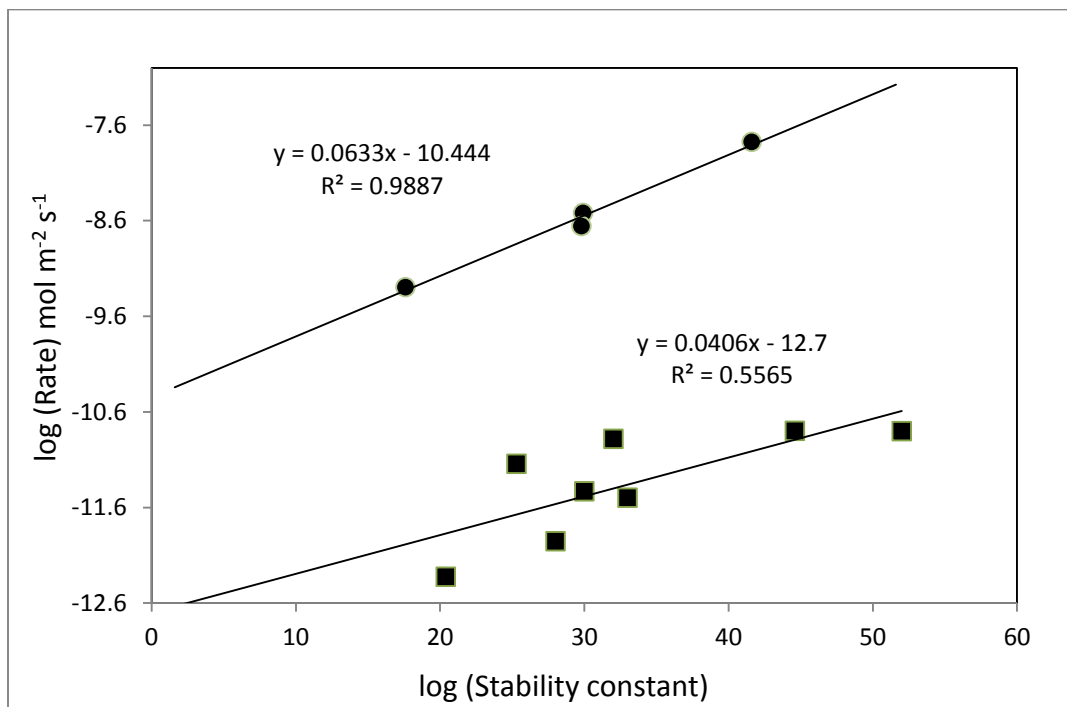


Figure 2.6. Plot of log stability constant and log dissolution rates of FeOOH (squares) and MnOOH (circles) as promoted by siderophores used in this study and from literature at pH 6. (Cocozaa, 2002; Neubauer, 2002; Lloyd 1999; Carrasco, 2009; Wolff-Boenisch and Traina, 2007; Reichard, 2007; Cervini-Silva, 2008; Harrington et al, 2012; Dubme et al., 1997).

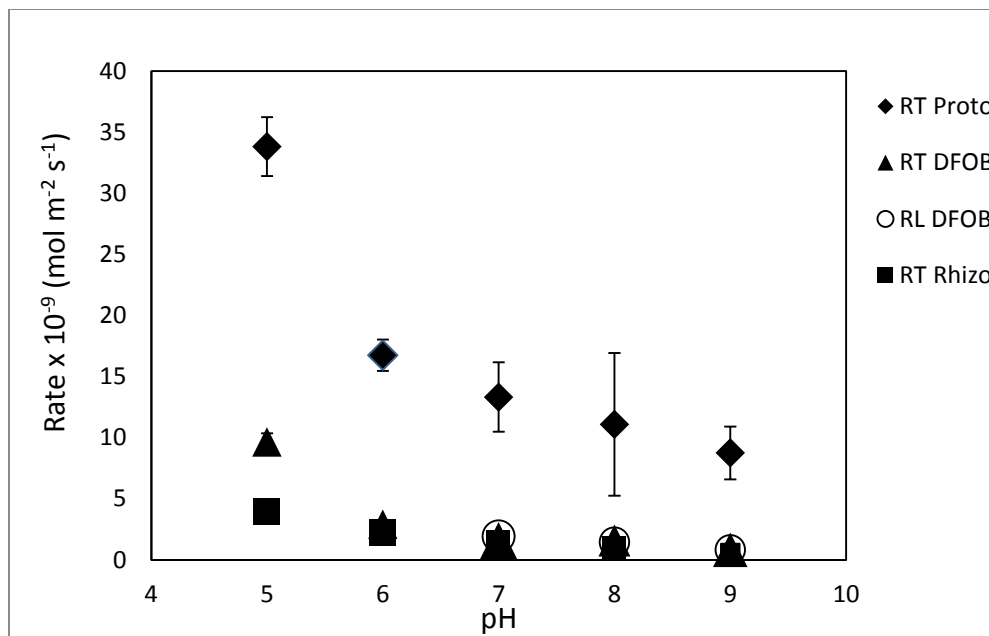


Figure 2.7. Average dissolution rates for MnOOH as promoted by DFOB, rhizoferrin, and protochelin. Conditions: 0.2 g L<sup>-1</sup> MnOOH; 100 μM siderophore; 25°C; 10 mM buffer; 0.1 M NaCl. Error bars represent 95% confidence interval.

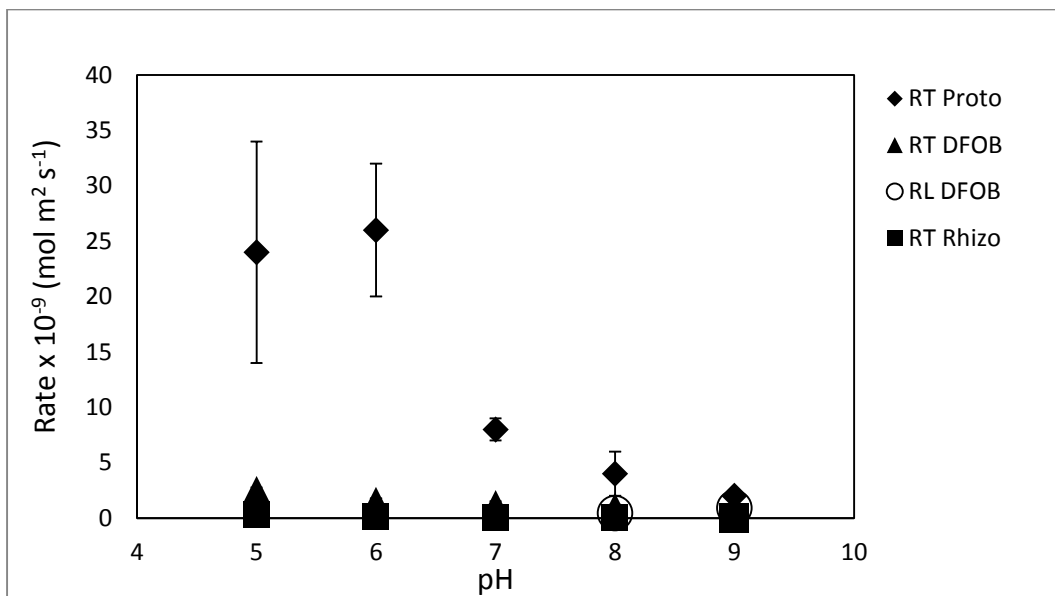


Figure 2.8. Average dissolution rates for CoOOH tested at 95% confidence interval as promoted by DFOB, rhizoferrin, and protochelin. Conditions: 0.2 g L<sup>-1</sup> CoOOH; 100 μM siderophore; 25°C; 10 mM buffer; 0.1 M NaCl.

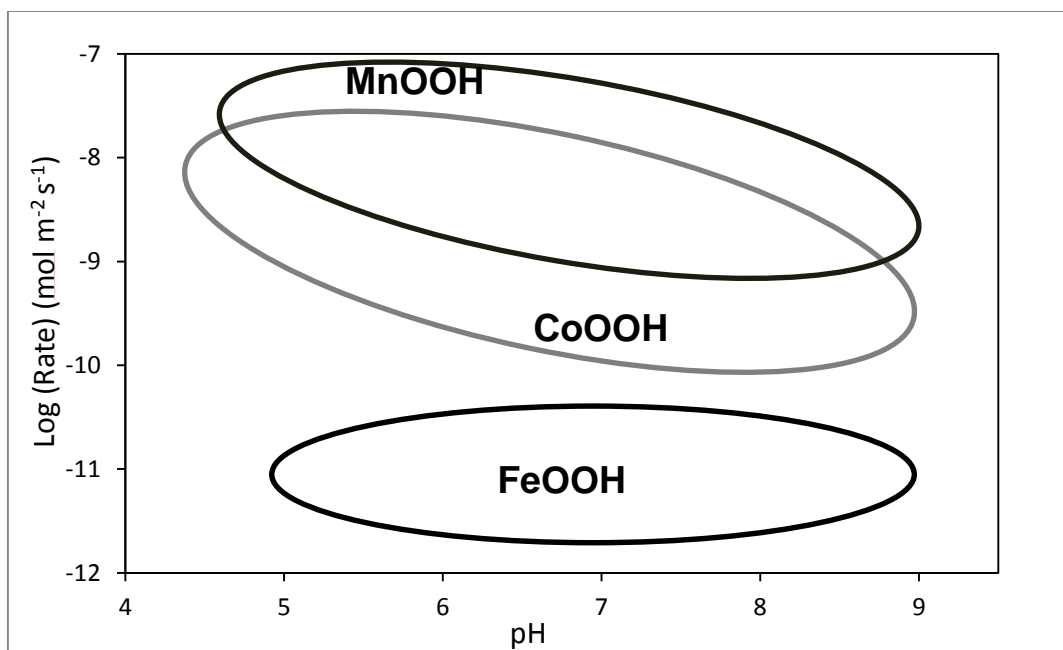


Figure 2.9. Trends in siderophore promoted dissolution rates for MnOOH, CoOOH and FeOOH as promoted by DFOB, rhizoferrin, and protochelin. MnOOH and CoOOH exceed FeOOH dissolution. Conditions: 0.2 g L<sup>-1</sup> CoOOH; 100 μM siderophore; 25°C; 10 mM buffer; 0.1 M NaCl

Table 2.2 Total dissolution ( $R_T$ ) and ligand-promoted ( $R_L$ ) dissolution rates for FeOOH. Conditions: 0.2 g L<sup>-1</sup> FeOOH; 100 μM siderophore; 25°C; 10 mM buffer; 0.1 M NaCl.

FeOOH dissolution rates / (mol m <sup>-2</sup> s <sup>-1</sup> ) × 10 <sup>11</sup>						
	DFOB		Rhizo		Proto	
pH	$R_T$	$R_L$	$R_T$	$R_L$	$R_T$	$R_L$
5	1.6 ± 0.4	1.6 ± 0.3	0.6 ± 0.1	0.6 ± 0.1	0.4 ± 0.2	0.4 ± 0.2
6	1.3 ± 0.3	1.3 ± 0.2	0.4 ± 0.1	0.6 ± 0.1	2 ± 1	1 ± 2
7	1.3 ± 0.1	1.3 ± 0.4	0.4 ± 0.1	0.5 ± 0.1	3 ± 1	2 ± 1
8	1.2 ± 0.4	1.2 ± 0.1	0.4 ± 0.2	0.5 ± 0.1	4 ± 1	6 ± 1
9	1.2 ± 0.2	1.2 ± 0.5	0.3 ± 0.1	0.5 ± 0.1	3.0 ± 0.2	7 ± 1

Table 2.3 Total initial dissolution rates ( $R_T$  in  $\text{mol m}^{-2} \text{s}^{-1}$ ) for FeOOH as promoted by DFOB and other siderophores at pH = 6.

Siderophore concentration ( $\mu\text{M}$ )	Siderophore	$\log(R_T)$	Reference
240	DFOB	-12.0	Cocozaa, 2002
100	DFOB	-12.4	Neubauer, 2002
100	DFOB	-12.1	Lloyd, 1999
80	DFOB	-12.2	Carrasco, 2009
100	DFOB	-10.9	This study
142	DFOB	-11.8	Wolff-Boenisch and Traina, 2007
100	Rhizoferrin	-11.1	This study
100	Protochelin	-10.8	This study
3000	DMA	-12.3	Reichard, 2007
240	DFOD <sub>1</sub>	-12.0	Cervini-Silva, 2008
240	DFOMTA	-11.5	Cervini-Silva, 2008
66	Enterobactin	-10.8	Wolff-Boenisch and Traina, 2007

Table 2.4 Total dissolution ( $R_T$ ) and ligand-promoted ( $R_L$ ) dissolution rates for MnOOH. Conditions: 0.2 g L<sup>-1</sup> MOOH; 100 μM siderophore; 25°C; 10 mM buffer; 0.1 M NaCl. ND = not detected.

MnOOH dissolution rates / (mol m <sup>-2</sup> s <sup>-1</sup> ) × 10 <sup>9</sup>				
	DFOB		Rhizo	Proto
pH	$R_T$	$R_L$	$R_T$	$R_T$
5	10.0 ± 0.7	ND	4 ± 1	34 ± 2
6	3.0 ± 0.2	ND	2.2 ± 0.3	17 ± 1
7	1.6 ± 0.2	1.9 ± 0.3	1.4 ± 0.2	13 ± 3
8	1.6 ± 0.2	1.5 ± 0.3	1.0 ± 0.1	11 ± 6
9	0.80 ± 0.04	0.8 ± 0.1	0.6 ± 0.1	9 ± 2

Table 2.5 Total dissolution ( $R_T$ ) and ligand-promoted ( $R_L$ ) dissolution rates for CoOOH. Conditions: 0.2 g L<sup>-1</sup> CoOOH; 100 μM siderophore; 25°C; 10 mM buffer; 0.1 M NaCl. ND = not detected.

CoOOH dissolution rates / (mol m <sup>-2</sup> s <sup>-1</sup> ) × 10 <sup>9</sup>				
	DFOB		Rhizo	Proto
pH	$R_T$	$R_L$	$R_T$	$R_T$
5	2.6 ± 0.1	ND	0.30 ± 0.04	24 ± 10
6	1.6 ± 0.2	ND	0.20 ± 0.03	26 ± 6
7	1.3 ± 0.2	ND	0.10 ± 0.01	8 ± 1
8	1.1 ± 0.1	0.4 ± 0.2	0.10 ± 0.01	4 ± 2
9	1.0 ± 0.1	0.9 ± 0.3	0.04 ± 0.01	2.0 ± 0.4

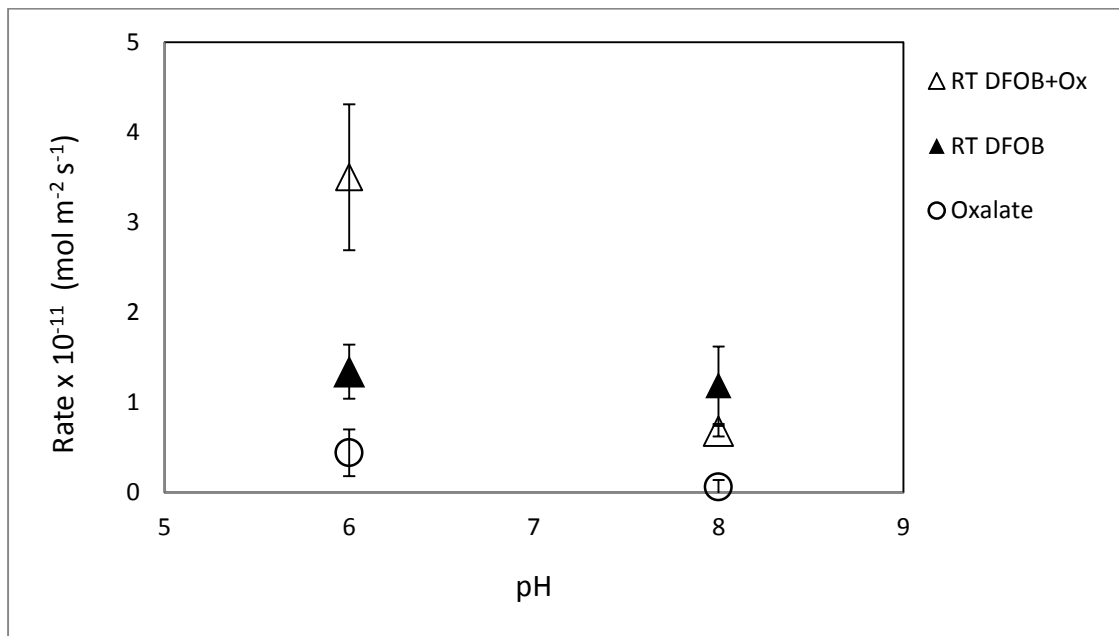


Figure 2.10. Average dissolution rates for FeOOH as promoted by DFOB with and without the presence of oxalate. Conditions:  $0.2 \text{ g L}^{-1}$  FeOOH;  $100 \text{ }\mu\text{M}$  siderophore;  $1000 \text{ }\mu\text{M}$  oxalate;  $25^\circ\text{C}$ ;  $10 \text{ mM}$  buffer;  $0.1 \text{ M}$  NaCl. Error bars represent 95% confidence intervals.

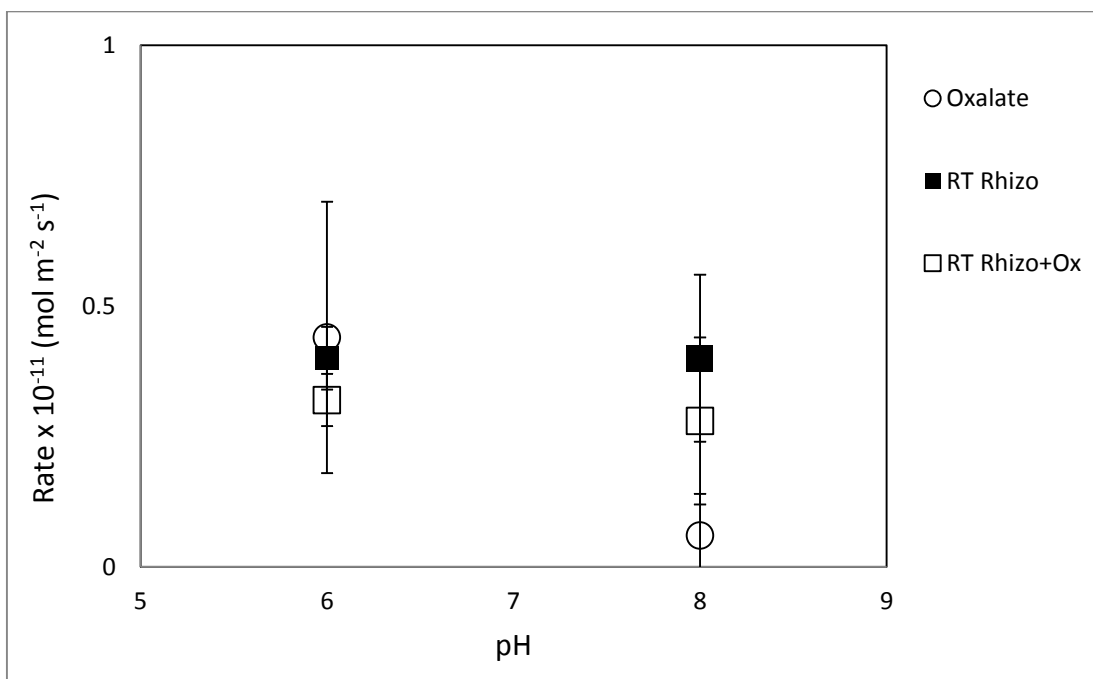


Figure 2.11. Average dissolution rates for FeOOH as promoted by rhizoferrin with and without the presence of oxalate. Conditions: 0.2 g L<sup>-1</sup> FeOOH; 100 μM siderophore; 1000 μM oxalate; 25°C; 10 mM buffer; 0.1 M NaCl. Error bars represent 95% confidence intervals.

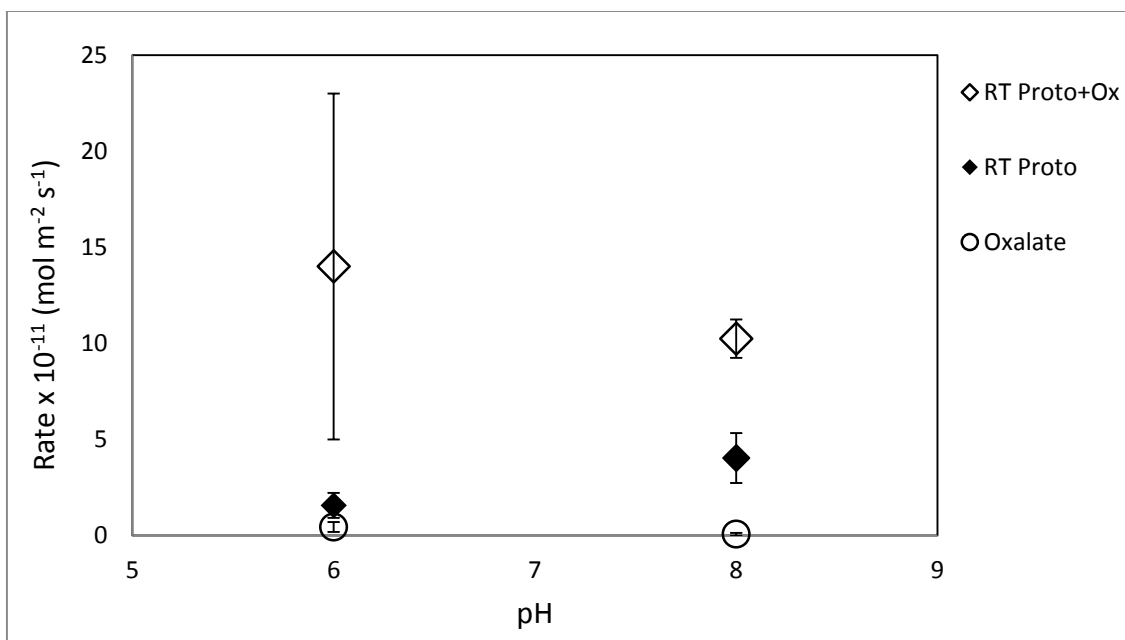


Figure 2.12. Average dissolution rates for FeOOH as promoted by protochelin with and without the presence of oxalate. Conditions: 0.2 g L<sup>-1</sup> FeOOH; 100 μM siderophore; 1000 μM oxalate; 25°C; 10 mM buffer; 0.1 M NaCl. Error bars represent 95% confidence intervals.

Table 2.6 Total siderophore-promoted ( $R_T$ ) dissolution rates for FeOOH, CoOOH, and MnOOH in the presence of oxalate ( $R_{Sox}$ ). Conditions: 0.2 g L<sup>-1</sup> MOOH; 100 μM siderophore; 0 or 1000 μM oxalate; 25°C; 10 mM buffer; 0.1 M NaCl.

FeOOH dissolution rates / (mol m <sup>-2</sup> s <sup>-1</sup> ) × 10 <sup>11</sup>							
Total dissolution rate ( $R_T$ )				Total dissolution rate in the presence of oxalate ( $R_{Sox}$ )			
pH	Proto	Rhizo	DFOB	Oxalate	Proto	Rhizo	DFOB
6	2.0 ± 1.0	0.3 ± 0.1	0.6 ± 0.2	0.4 ± 0.3	14.0 ± 9.0	0.3 ± 0.1	4.0 ± 1.0
8	4.0 ± 1.3	0.3 ± 0.1	1.5 ± 0.2	0.1 ± 0.1	10.0 ± 4.0	0.3 ± 0.1	0.7 ± 0.1

MnOOH dissolution rates / (mol m <sup>-2</sup> s <sup>-1</sup> ) × 10 <sup>9</sup>							
Total dissolution rate ( $R_T$ )				Total dissolution rate in the presence of oxalate ( $R_{Sox}$ )			
pH	Proto	Rhizo	DFOB	Oxalate	Proto	Rhizo	DFOB
6	17.0 ± 1.3	2.0 ± 0.3	3.0 ± 0.2	0.8 ± 0.3	27.2 ± 6.1	2.1 ± 0.3	3.2 ± 0.2
8	11.0 ± 6.0	1.0 ± 0.1	1.6 ± 0.2	0.3 ± 0.2	9.3 ± 7.3	1.0 ± 0.3	1.0 ± 0.1

CoOOH dissolution rates / (mol m <sup>-2</sup> s <sup>-1</sup> ) × 10 <sup>-9</sup>							
Total dissolution rate ( $R_T$ )				Total dissolution rate in the presence of oxalate ( $R_{Sox}$ )			
pH	Proto	Rhizo	DFOB	Oxalate	Proto	Rhizo	DFOB
6	26 ± 6	0.2 ± 0.03	2.0 ± 0.2	0.2 ± 0.1	14 ± 6	0.3 ± 0.1	1.0 ± 0.1
8	4 ± 2	0.1 ± 0.01	1.0 ± 0.1	0.03 ± 0.02	6 ± 3	0.10 ± 0.01	1.0 ± 0.2

Table 2.7 Enhanced siderophore promoted total dissolution rates for FeOOH, CoOOH, and MnOOH in the presence of oxalate ( $R_{Sox}$ ). Conditions: 0.2 g L<sup>-1</sup> MOOH; 0 or 100 μM siderophore; 1000 μM oxalate; 25°C; 10 mM buffer; 0.1 M NaCl.

FeOOH	Oxalate promoted increase in dissolution		
pH	Proto	Rhizo	DFOB
6	9x	0	3x
8	3x	0	0
CoOOH			
pH	Proto	Rhizo	DFOB
6	0	2x	0
8	2x	0	0
MnOOH			
pH	Proto	Rhizo	DFOB
6	2x	0	0
8	0	0	0

## **Chapter 3**

### **Summary and Conclusions**

### 3.1 Summary of Findings

The work in this thesis focused on the measuring the initial dissolution rates of FeOOH, CoOOH, and MnOOH as promoted by the siderophores DFOB, rhizoferrin, and protochelin in the presence or absence of oxalate by using batch experiments. By utilizing UV-visible and atomic absorption spectroscopy, we were able to measure in most cases both the ligand dissolution and total dissolution pathways promoted by siderophores for each mineral.

Our findings showed that dissolution rate for FeOOH was the slowest, followed by CoOOH and MnOOH. For CoOOH and MnOOH, total dissolution rates ( $R_T$ ) showed a similar trend for all three siderophores, decreasing with increasing pH for all three siderophores, with protochelin  $\gg$  rhizoferrin  $\approx$  DFOB. For FeOOH, the protochelin-promoted dissolution rate was greater than for DFOB, which was greater than for rhizoferrin; however, protochelin-promoted dissolution rates increased with pH, whereas DFOB and rhizoferrin-promoted dissolution were pH independent. For FeOOH, only ligand-promoted dissolution occurred over the pH range of study (pH = 5-9). For MnOOH and CoOOH however, we only observed ligand-promoted dissolution by DFOB at pH  $> 6$  for MnOOH and at pH  $> 7$  for CoOOH.

We also observed that with oxalate added as a precursor to siderophore addition at pH = 6, dissolution was greatly enhanced for protochelin and DFOB. However, at pH = 8 the effect was inhibited, implying that synergistic effects of low molecular mass organic acids are dependent on pH as well as siderophore identity. Given the general instability of protochelin (Harrington et al., 2012) at pH  $> 7$  (most siderophores are thought to be relatively short-lived in the environment (Reichard et al., 2007)) as well as the relatively slow siderophore-promoted dissolution rates of FeOOH, the enhancement of the dissolution rates by the presence of oxalate

suggests that different siderophores and low molecular mass organic acids may be secreted together to ensure optimum nutrient solubilization and uptake.

### **3.2 Broader Implications of Major Findings**

The dissolution process involving metal hydroxides is particularly important because, in addition to providing nutrients for microbes and other organisms, they comprise a large proportion of reactive surface area in soil or mineral surfaces (Penn et al., 2001). My work in this thesis shows that that under similar environmental conditions, siderophores react differently with metal hydroxides, depending on their functional groups as well as the type of metal. The difference in reactivity at different pH implies that siderophores may be playing other roles in the environment. For example, because Fe often occurs associated with Mn (Burns, 1976; McDaniel and Buol, 1991), it is possible that reductive dissolution of Mn (and Co) at  $\text{pH} < 7$  by siderophores could serve as a sink to remove unwanted siderophores or disrupt microbial uptake of iron. The varying strengths of the siderophore-metal complex may be related to their relative abundance in the Earth's crust and that the varying dissolution rates of different metals with different siderophores could be directly related to the nutritional requirements as well as method of nutrient uptake by different organisms. It is also possible that production of siderophores is an adaptation by nature to obtain important nutrients. Their different structures could reflect diversity of organisms and that low molecular mass organic acids work differently with siderophores to sometimes enhance or suppress the dissolution of metal hydroxides of less stable siderophores.

The knowledge that we have gained about the ability of siderophores to form soluble complexes with metal ions can be applied in the remediation of metal contaminated ground water and soil. Although current methods of synthesis of siderophores are quite expensive, with the ever improving methods, cheaper analogs could be made in commercial quantities or that microbes could genetically be modified to produce siderophores that could be applied to solubilize toxic metals out of the soil for uptake by plants as an environmentally friendly method for the cleanup of metal impacted sites. Solubilized metals could also serve as an energy source for microbes that have been adapted to the conditions of these sites.

### **3.3 Final Thoughts**

Additional work and different approaches may support and enhance the results of this work. Because the precursor to dissolution is adsorption, experiments on the adsorption of siderophores as well as oxalate to metal hydroxides would have further elucidated reaction mechanisms, especially the synergistic effect of oxalate at higher pH. Quantification of breakdown products of protochelin at pH 7-9, using mass spectrometry or nuclear magnetic resonance spectroscopy, could have helped understand the reaction mechanism of protochelin at higher pH and provided more insight into why the synergistic effect of oxalate added as a precursor to the siderophore was higher for protochelin and DFOB but not for rhizoferrin. It is also possible that complexes of Co and Mn were formed at  $\text{pH} > 7$  for protochelin and rhizoferrin but were too short-lived to measure. Given that all the metal hydroxides under consideration were all redox active, measurement of electrode potential during the course of the experiment would have provided more information about the true conditions of the

experimental conditions and a better understanding of the state and speciation of the metal hydroxides.

Work presented here fills a knowledge gap about the interaction of different siderophores each with different functional groups with a range of different metal hydroxides. A direction for future work would be to investigate the dissolution mechanism of the same metal hydroxides with pyroverdin CFML90-51, a bacterial siderophore that has all the three functional groups (Boukhalfa et al., 2006), to probe if there is a preferential dissolution of metal hydroxides by functional groups based on the dissolution rates that we observed in the work just completed. A further probing of surface properties of metal hydroxides during dissolution would give more insight about the effect of oxalate on siderophore dissolution at high pH.

### 3.4 References

1. Boukhalfa, H., Reilly, S.D., Michalczyk, R., Iyer, S., Neu, M.P., 2006. Iron (III) coordination properties of a pyoverdine siderophore produced by *Pseudomonas putida* ATCC 33015. *Inorganic chemistry* 45, 5607-5616.
2. Burns, R.G., 1976. The uptake of cobalt into ferromanganese nodules, soils, and synthetic manganese (IV) oxides. *Geochimica et Cosmochimica Acta* 40, 95-102.
3. Harrington, J.M., Parker, D.L., Bargar, J.R., Jarzecki, A.A., Tebo, B.M., Sposito, G., Duckworth, O.W., 2012. Structural dependence of Mn complexation by siderophores: Donor group dependence on complex stability and reactivity. *Geochimica et Cosmochimica Acta* 88, 106-119.
4. McDaniel, P., Buol, S., 1991. Manganese distributions in acid soils of the North Carolina Piedmont. *Soil Science Society of America Journal* 55, 152-158.
5. Penn, R.L., Stone, A.T., Veblen, D.R., 2001. Defects and disorder: Probing the surface chemistry of heterogenite (CoOOH) by dissolution using hydroquinone and iminodiacetic acid. *The Journal of Physical Chemistry B* 105, 4690-4697.
6. Reichard, P.U., Kretschmar, R., Kraemer, S.M., 2007. Dissolution mechanisms of goethite in the presence of siderophores and organic acids. *Geochimica et Cosmochimica Acta* 71, 5635-5650.

## **APPENDIX**

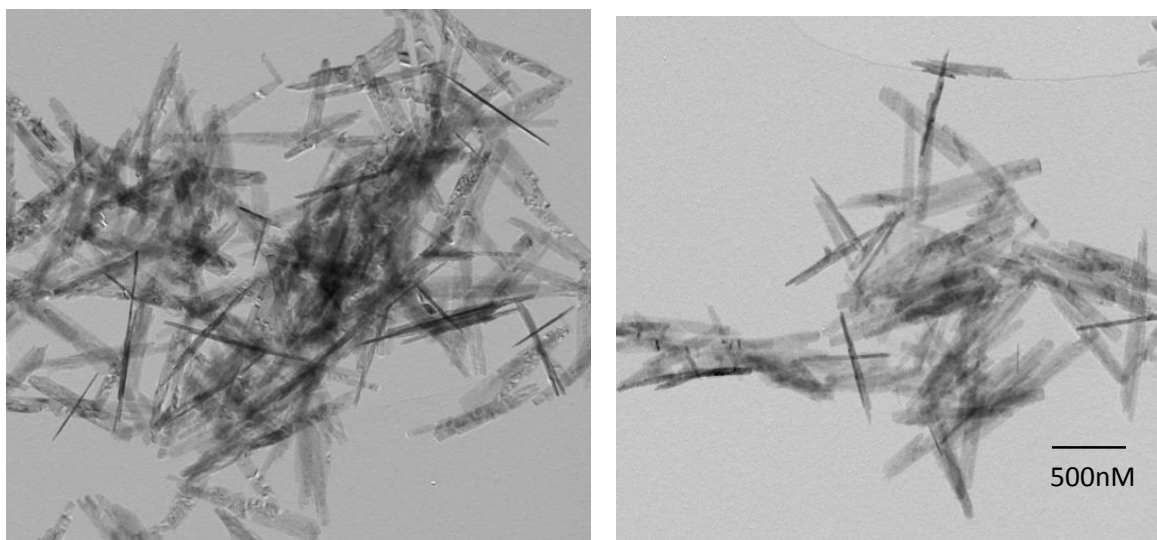
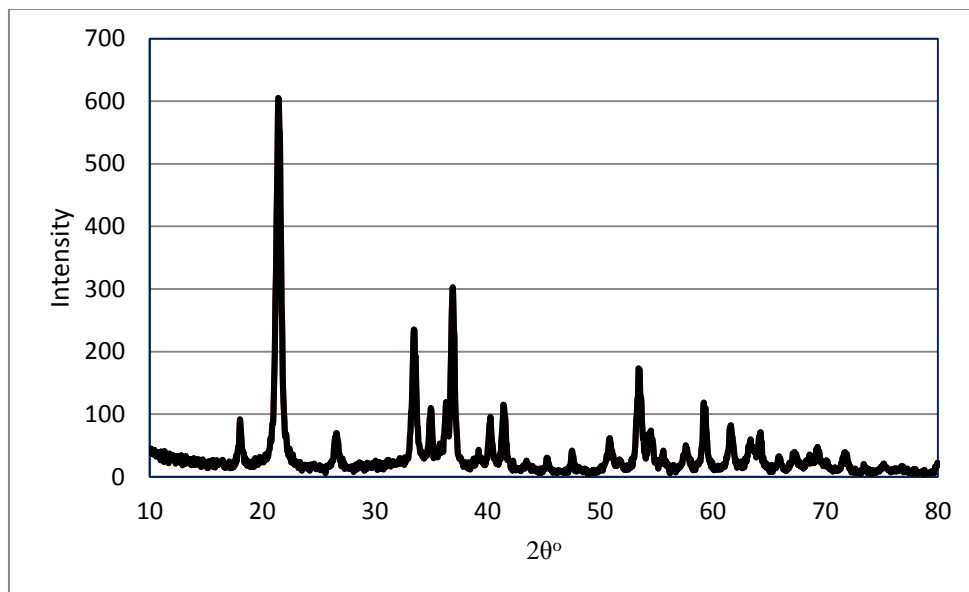


Figure A2.1 Transmission electron micrograph (TEM) at 6000× magnification and X-ray diffractogram of synthetic FeOOH.

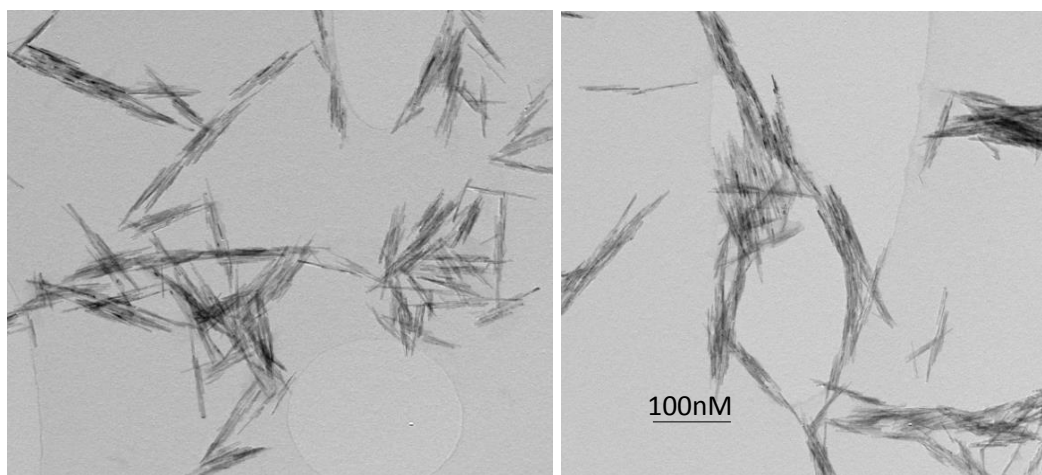
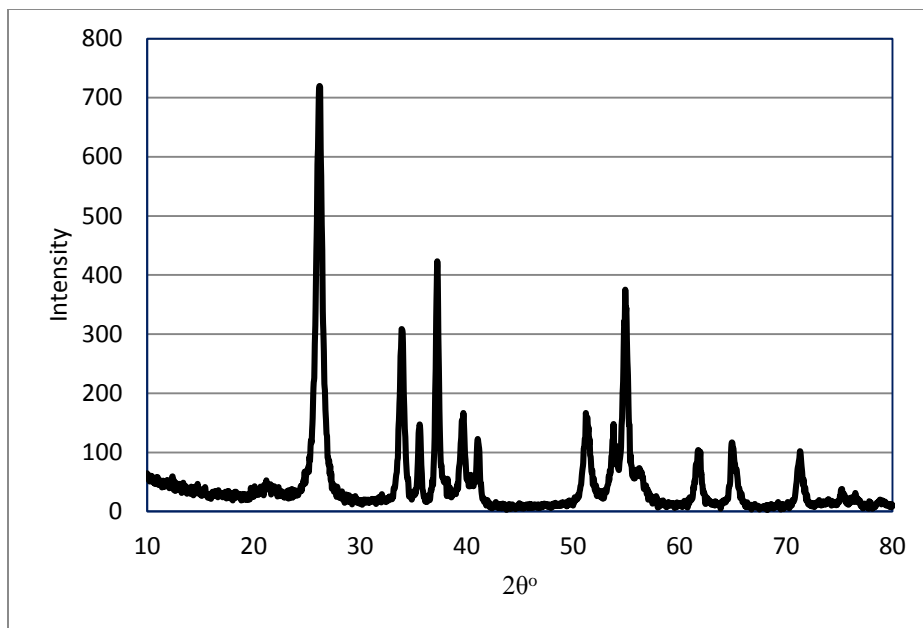


Figure A2.2 Transmission electron micrograph (TEM) at 6000× magnification and X-ray diffractogram of synthetic MnOOH.

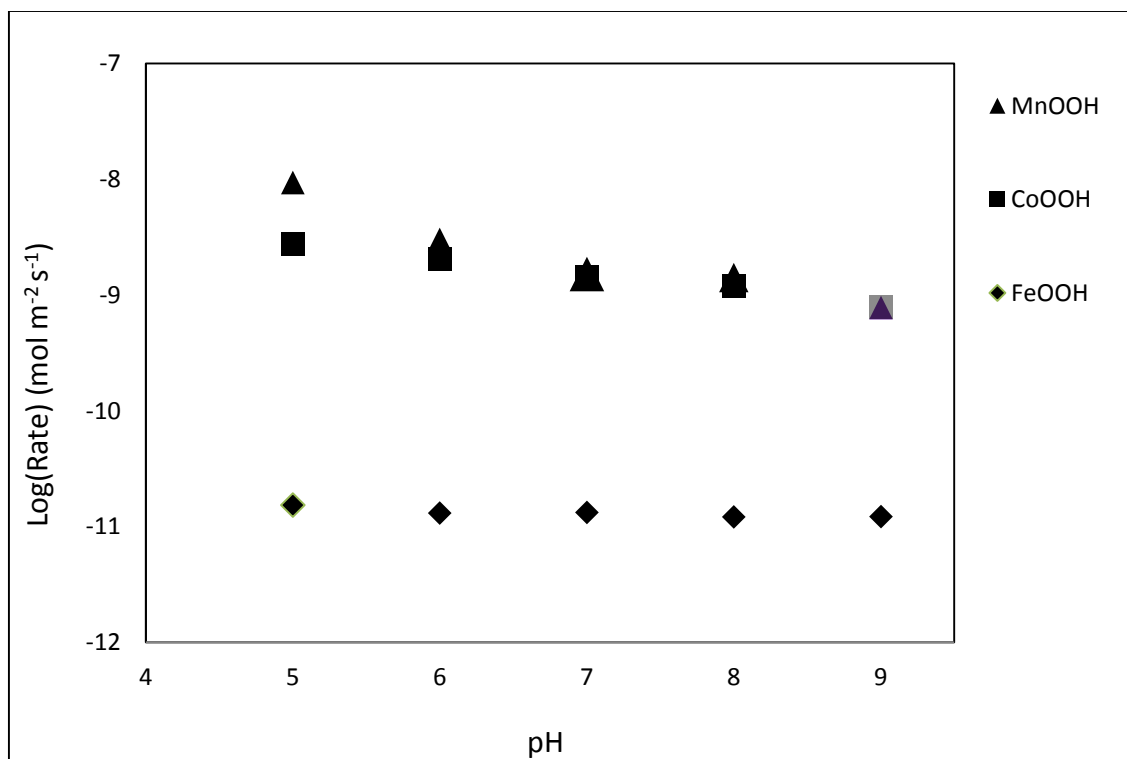


Figure A2.3 Average dissolution rates for metal hydroxides as promoted by DFOB. Conditions: 0.2 g L<sup>-1</sup> FeOOH, MnOOH, CoOOH; 100  $\mu$ M siderophore; 25°C; 10 mM buffer; 0.1 M NaCl.

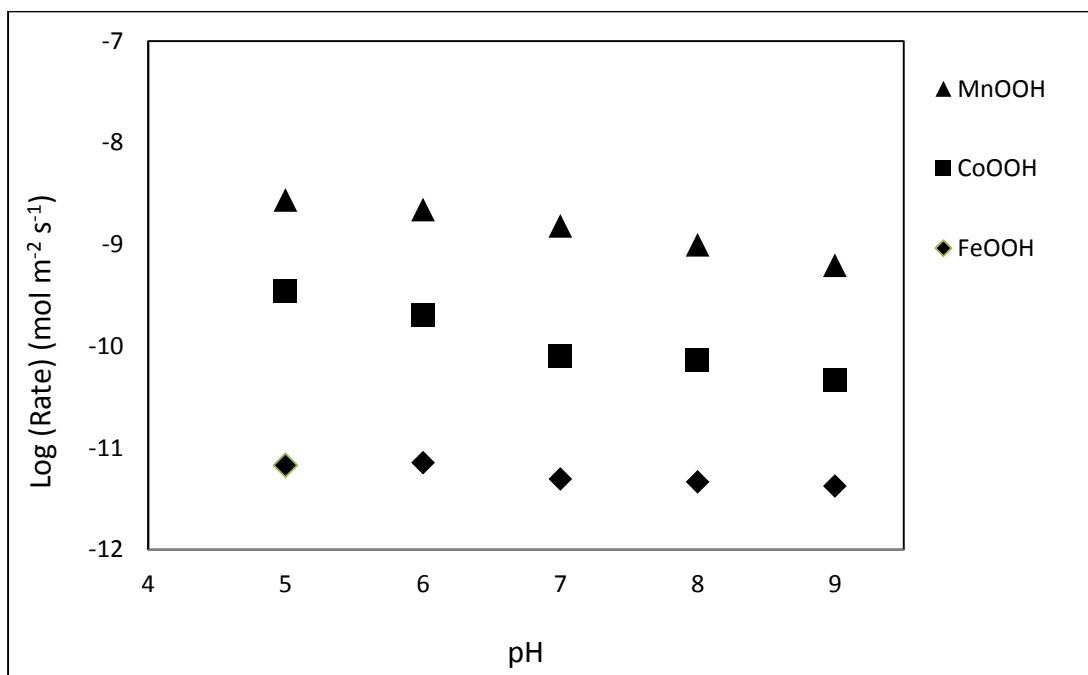


Figure A2.4 Average dissolution rates for metal hydroxides as promoted by rhizoferrin. Conditions: 0.2 g L<sup>-1</sup> FeOOH, MnOOH, CoOOH; 100 μM siderophore; 25°C; 10 mM buffer; 0.1 M NaCl.

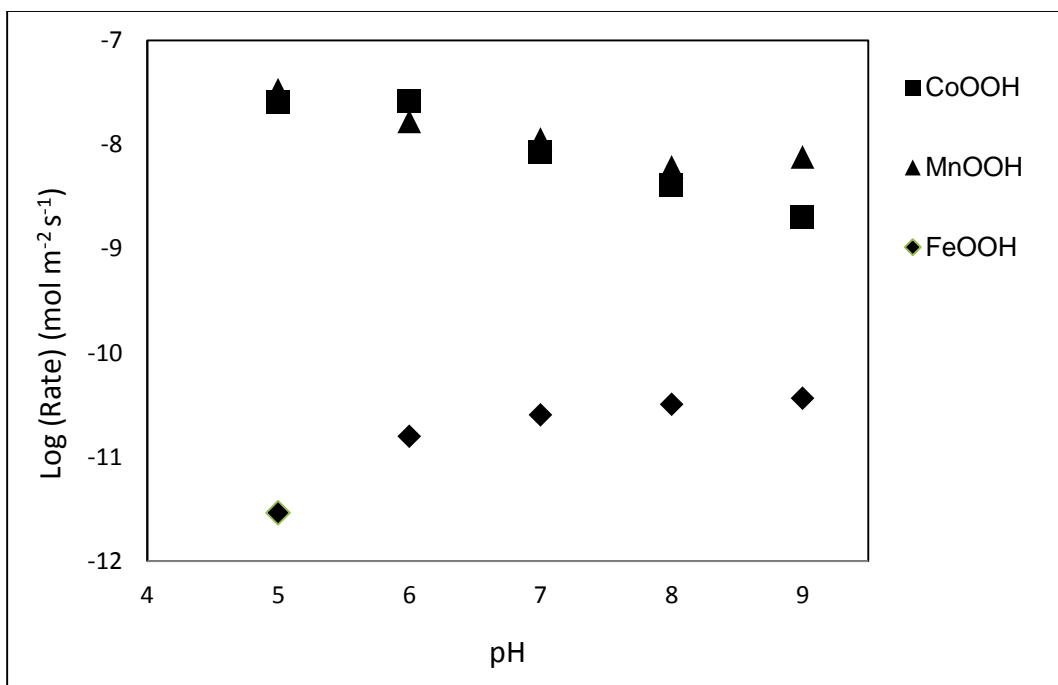


Figure A2.5 Average dissolution rates for metal hydroxides as promoted by protochelin. Conditions: 0.2 g L<sup>-1</sup> FeOOH, MnOOH, CoOOH; 100 μM siderophore; 25°C; 10 mM buffer; 0.1 M NaCl.

Co(III)-rhizoferrin was prepared based on a procedure to produce DFOB (Duckworth et al., 2009). A stoichiometric concentration of  $\text{CoCl}_2$  and rhizoferrin were dissolved in in 40% glycerol. Excess 3% hydrogen peroxide was added. The pH was adjusted to  $\text{pH} = 8.5$  using 0.1 M NaOH. The solution was heated for 1 hr as it turned from pink to green. The final concentration is 4 mM.

Co K-edge fluorescence-yield (FY) spectra of a solutions containing 4 mM Co(III)Rhizoferrin were measured at Stanford Synchrotron Radiation Lightsource (SSRL) Beamline 11-2 using a 30 element Ge fluorescence detector and a liquid helium cryostat (7-10° K). Multiple spectra were collected for each sample, with no evidence of beam damage in successive scans, and averaged to improve the signal-to-noise ratio. The incident beam was detuned to 30% and monochromatized using a variable-exit Si(220) double-crystal monochromator, and rhodium-coated mirrors were used to reject harmonics. In all cases, spectra were collected using Soller slits and a Fe X-ray filter to improve the signal-to-noise ratio. Spectra were calibrated by adjusting the  $E_0$  of a Co foil to 7709 eV The spectrum was dead-time corrected, energy calibrated, averaged, background-subtracted, splined, and fit in  $R$ -space (Kelly et al., 2008) using the SIXPACK interface (Webb, 2005), which makes use of the IFEFFIT code (Newville, 2001).

To facilitate comparison with previous work, a five shell model based on fits of other rhizoferrin complexes (Harrington et al., 2012), was also utilized to fit the model. Amplitude and phase functions were calculated from atomic positions the optimized Fe Protochelin DFT with Co substituted for Fe structure using FEFF 9. The  $S_0^2$ ,  $\Delta E_0$ ,  $\sigma^2$ , and  $R$  were treated in the same manner in the three shell model. For the first shell,  $N$  was allowed to float whereas  $N =$

6 for the second shell carbon, and third shell fit. A shell with two oxygen atoms was used to fit distal carboxylate oxygens and a triangular three-legged multiple scattering path containing 12 cobalt–carbon–oxygen was also included.

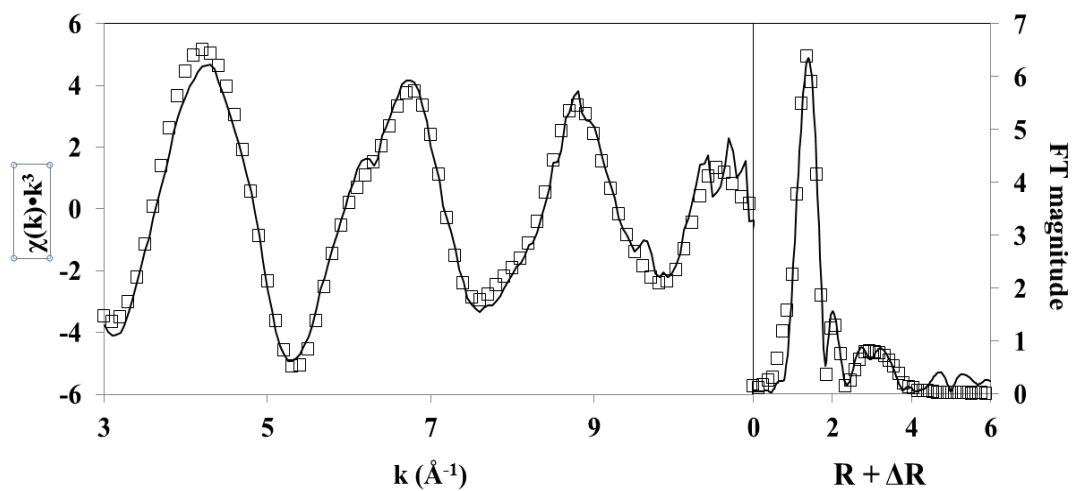


Figure A2.6. K-edge Co EXAFS spectrum of the Co(III)-Rhizoferrin<sup>3-</sup> complex. Solid lines indicate experimental data, whereas points indicate the fit of a structural model. The optimized parameters used to produce the fit are shown in Table A2.1.

Table A2.1 Amplitude reduction factors, coordination numbers, interatomic distances, and Debye-Waller factors Co(III)-Rhizoferrin<sup>a</sup>

Ligand	$S_0^2$	First Shell M-O			Second Shell M-C			Third Shell M-C			Multiple Scattering M-C-O		
		N	R (Å)	$\sigma^2$ (Å <sup>2</sup> )	N	R (Å)	$\sigma^2$ (Å <sup>2</sup> )	N	R (Å)	$\sigma^2$ (Å <sup>2</sup> )	N	R (Å)	$\sigma^2$ (Å <sup>2</sup> )
Co(III)Rhizo	0.84 <sup>b</sup>	6[1]	1.85[1]	0.010[1]	6 <sup>c</sup>	2.41[4]	0.020[6]	6 <sup>c</sup>	3.93[3]	0.008[2]	12 <sup>c</sup>	2.75[2]	0.001[2]
					2 <sup>c</sup>	3.09[2]	0.004[2]						

(a) Numbers in brackets represent uncertainty of the last decimal place of their respective values; (b) Duckworth et al., 2009; (c) Fixed coordination number.

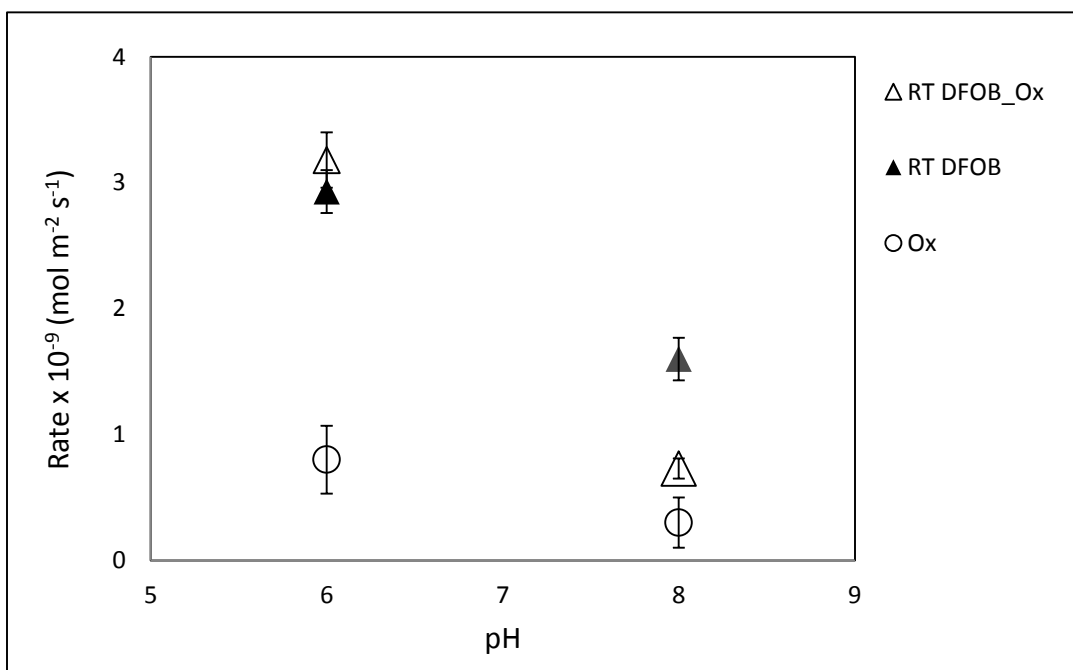


Figure A2.7. Average dissolution rates for MnOOH as promoted by DFOB with and without the presence of oxalate. Conditions: 0.2 g L<sup>-1</sup> MnOOH; 100 μM siderophore; 1000 μM oxalate; 25°C; 10 mM buffer; 0.1 M NaCl. Error bars represent 95% confidence intervals.

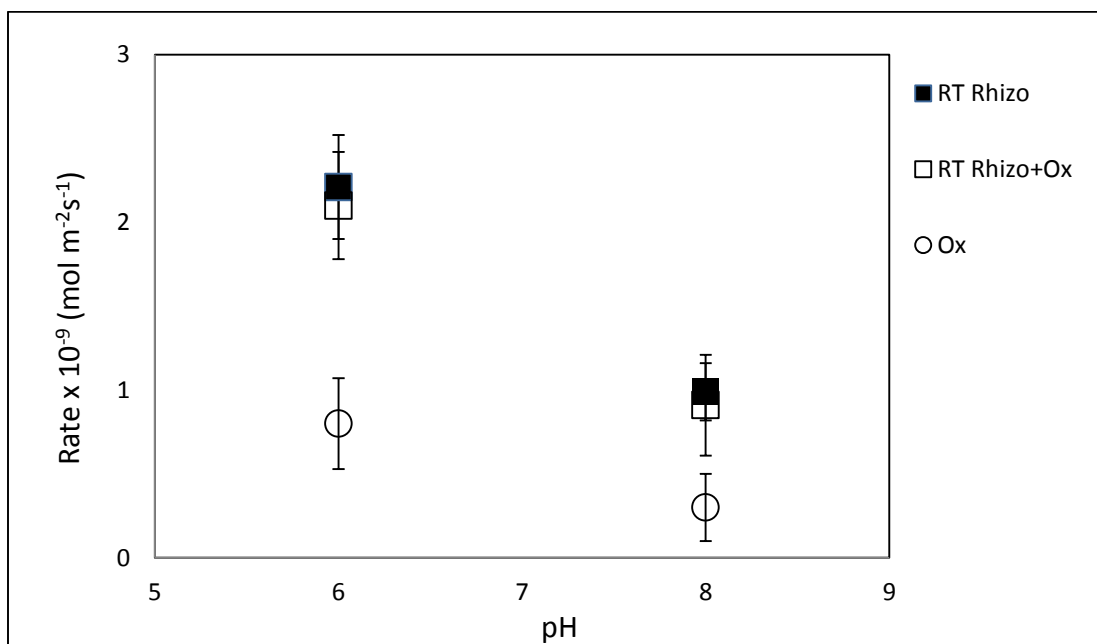


Figure A2.8. Average dissolution rates for MnOOH as promoted by rhizoferrin with and without the presence of oxalate. Conditions:  $0.2 \text{ g L}^{-1}$  MnOOH;  $100 \text{ }\mu\text{M}$  siderophore;  $1000 \text{ }\mu\text{M}$  oxalate;  $25^\circ\text{C}$ ;  $10 \text{ mM}$  buffer;  $0.1 \text{ M}$  NaCl. Error bars represent 95% confidence intervals.

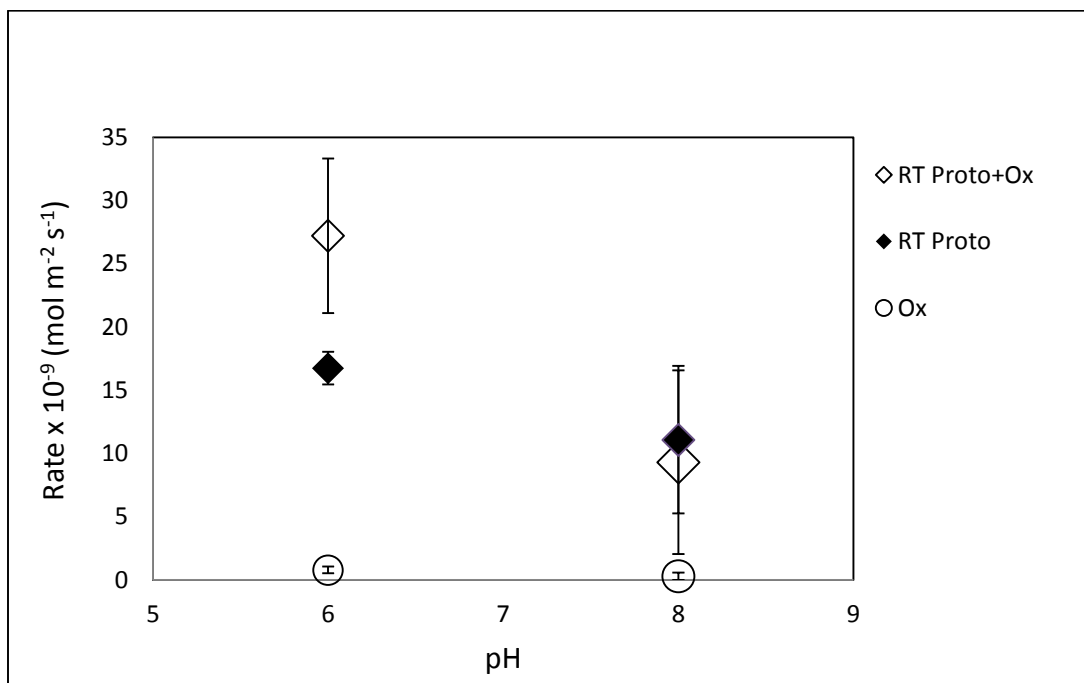


Figure A2.9. Average dissolution rates for MnOOH as promoted by protochelin with and without the presence of oxalate. Conditions: 0.2 g L<sup>-1</sup> MnOOH; 100  $\mu$ M siderophore; 1000  $\mu$ M oxalate; 25°C; 10 mM buffer; 0.1 M NaCl. Error bars represent 95% confidence intervals.

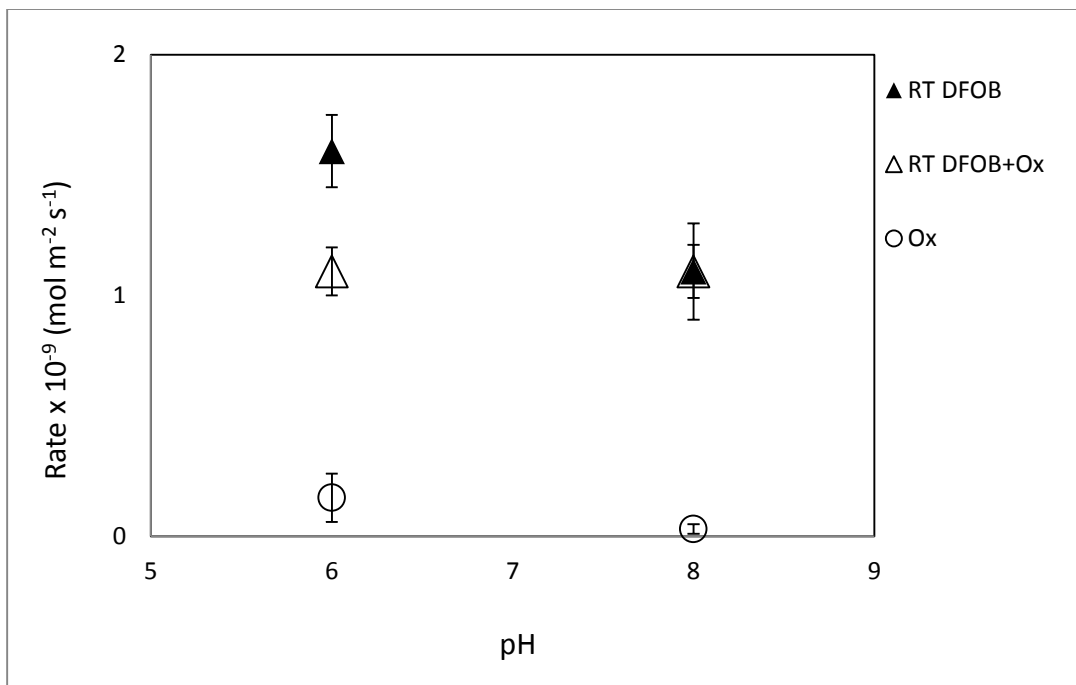


Figure A2.10. Average dissolution rates for CoOOH as promoted by DFOB with and without the presence of oxalate. Conditions: 0.2 g L<sup>-1</sup> CoOOH; 100 μM siderophore; 1000 μM oxalate; 25°C; 10 mM buffer; 0.1 M NaCl.

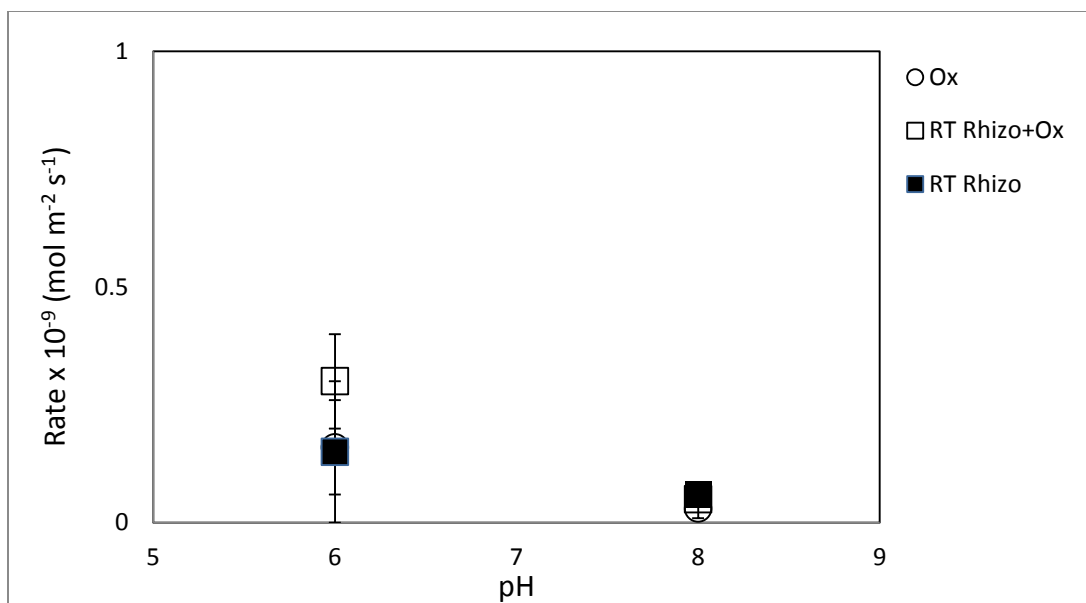


Figure A2.11. Average dissolution rates for CoOOH as promoted by rhizoferrin with and without the presence of oxalate. Conditions: 0.2 g L<sup>-1</sup> CoOOH; 100 μM siderophore; 1000 μM oxalate; 25°C; 10 mM buffer; 0.1 M NaCl.

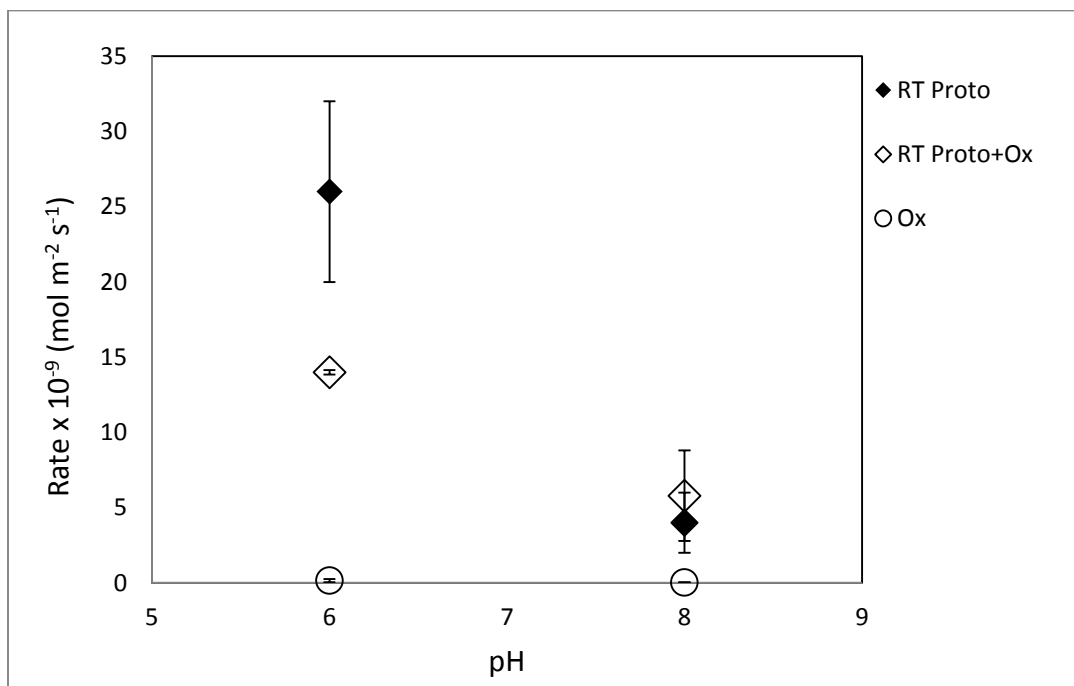


Figure A2.12. Average dissolution rates for CoOOH as promoted by protochelin with and without the presence of oxalate. Conditions:  $0.2 \text{ g L}^{-1}$  CoOOH;  $100 \text{ }\mu\text{M}$  siderophore;  $1000 \text{ }\mu\text{M}$  oxalate;  $25^\circ\text{C}$ ;  $10 \text{ mM}$  buffer;  $0.1 \text{ M}$  NaCl.